Research Paper

Multi omics analysis of mitophagy subtypes and integration of machine learning for predicting immunotherapy responses in head and neck squamous cell carcinoma

Junzhi Liu[1,*], Huimin Li[2,*], Qiuping Dong[2], Zheng Liang[1]

[1]Department of Otorhinolaryngology, Tianjin Medical University General Hospital, Tianjin 300052, China
[2]Laboratory of Cancer Cell Biology, National Clinical Research Center for Cancer, Key Laboratory of Cancer Immunology and Biotherapy, Tianjin's Clinical Research Center for Cancer, Tianjin Medical University Cancer Institute and Hospital, Tianjin, China
*Equal contribution

Correspondence to: Zheng Liang; **email:** liangzheng01@tmu.edu.cn
Keywords: mitophagy, single cell, machine learning, immunotherapy response, immune microenvironment
Received: December 12, 2023 **Accepted:** March 29, 2024 **Published:** June 21, 2024

Copyright: © 2024 Liu et al. This is an open access article distributed under the terms of the Creative Commons Attribution License (CC BY 4.0), which permits unrestricted use, distribution, and reproduction in any medium, provided the original author and source are credited.

ABSTRACT

Mitophagy serves as a critical mechanism for tumor cell death, significantly impacting the progression of tumors and their treatment approaches. There are significant challenges in treating patients with head and neck squamous cell carcinoma, underscoring the importance of identifying new targets for therapy. The function of mitophagy in head and neck squamous carcinoma remains uncertain, thus investigating its impact on patient outcomes and immunotherapeutic responses is especially crucial. We initially analyzed the differential expression, prognostic value, intergene correlations, copy number variations, and mutation frequencies of mitophagy-related genes at the pan-cancer level. Through unsupervised clustering, we divided head and neck squamous carcinoma into three subtypes with distinct prognoses, identified the signaling pathway features of each subtype using ssGSEA, and characterized subtype B as having features of an immune desert using various immune infiltration calculation methods. Using multi-omics data, we identified the genomic variation characteristics, mutated gene pathway features, and drug sensitivity features of the mitophagy subtypes. Utilizing a combination of 10 machine learning algorithms, we have developed a prognostic scoring model called Mitophagy Subgroup Risk Score (MSRS), which is used to predict patient survival and the response to immune checkpoint blockade therapy. Simultaneously, we applied MSRS to single-cell analysis to explore intercellular communication. Through laboratory experiments, we validated the biological function of SLC26A9, one of the genes in the risk model. In summary, we have explored the significant role of mitophagy in head and neck tumors through multi-omics data, providing new directions for clinical treatment.

INTRODUCTION

HNSCC, also known as head and neck squamous cell carcinoma, accounts for 95% of cancerous growth in the head and neck area, resulting in over 316,000 deaths worldwide annually [1, 2]. Similar to other forms of solid cancers, HNSCC encounters various obstacles during its progression, such as oxygen deprivation, inadequate nourishment, immune cell toxicity, and diverse treatment modalities [3, 4]. Maintaining a functional network of mitochondria in tumors relies heavily on the process of mitophagy, which is responsible for selectively eliminating malfunctioning mitochondria [5–7]. The resultant decomposition byproducts can function as bioenergetic intermediaries to facilitate unimpeded expansion. In HNSCC, targeting mitophagy in different

signaling pathways has been found to prevent oncogenesis [8–10]. Hence, it is beneficial to investigate the importance of mitophagy in HNSCC, as it aids in comprehending the processes of tumor development and aiming at malignant proliferation.

Mitophagy, a selective form of autophagy confined to the mitochondria, targets the elimination of damaged and senescent mitochondria, significantly impacting the maintenance of cellular mitochondrial quantity and quality [11, 12]. This process is crucial in regulating the balance of cancer cells, where it can function to promote or suppress cancerous growth. Although mitophagy acts as a defense against various environmental insults by preserving mitochondrial integrity and energy homeostasis, its dysregulation can contribute to mitochondrial network abnormalities and energy production disruptions, influencing cancer development and progression [13, 14]. The activation of mitophagy can vary with cell types, involving different pathways like PINK1/Parkin, BNIP3/Nix, and FUNDC1 [11]. In cancer cells, mitophagy has a dual effect, serving as a tumor promoter or inhibitor. Initially, by clearing defective mitochondria, it protects cells from oxidative and DNA damage, potentially preventing tumor initiation. However, in established tumors, especially those that are advanced or aggressive, cancer cells harness mitophagy to alleviate oxidative stress and recycle components for growth and survival [15–17]. Mitophagy's connection with cancer cell metabolic reprogramming, drug resistance, and stem-like properties is well-established. Key pathways, including the classic PINK1-Parkin and the hypoxia-driven BNIP3/Nix and FUNDC1 pathways, are implicated in the metabolic reconfiguration of cancer cells, particularly affecting glycolysis. In the absence of Parkin, PTEN degradation occurs, modulating glycolysis and activating PI3K/AKT signaling through Parkin-PTEN interactions [18]. Furthermore, the PINK1-Parkin pathway can trigger a HIF1α-dependent Warburg effect, which is a hallmark of cancer metabolism, by degrading mitochondrial transporters SLC25A37 and SLC25A28. This leads to an accumulation of mitochondrial iron, supporting the relentless division and growth of cancer cells [19].

The development of cancer is frequently associated with the initiation of oncogenic signals and an adjustment to low oxygen environments. It is observed that Parkin inhibits glycolysis by binding with pyruvate kinase M2 (PKM2) and facilitating the ubiquitination and subsequent breakdown of HIF1a. This action hampers the stimulation of proteins that promote glycolysis and various transcriptional targets [20]. In a similar vein, the lack of PINK1 correlates with the Warburg effect, which is marked by the stabilization of HIF1a and a reduction in PKM2 efficacy [21]. Disruption of essential elements of the mitophagy pathway can result in its dysfunction. Conversely, a rise in mitochondrial ROS is documented to transcriptionally heighten HIF1a, triggering the metabolism of glycolysis and the expression of its associated genes (BNIP3, NIX, FUNDC1), thereby influencing mitophagy [22]. Research indicates that mitophagy plays a crucial role in sustaining stem cell reserves, including those traits that are stem-like within cancer stem cells (CSCs) [23–26]. There is a strong connection between mitophagy and cellular adaptability. Notably, a metabolic shift induced by mitophagy from glycolysis to oxidative phosphorylation enhances the stemness characteristics of CSCs [27]. CSCs undergo specific metabolic changes governed by mitochondrial dynamics, shaped by the cellular microenvironment. It has been documented that mitochondrial function contributes to the metabolic reprogramming of CSCs in nasopharyngeal carcinoma [28]. The switch from oxidative phosphorylation to glycolysis is critical for bolstering the stem-like qualities of CSCs. Additionally, mitophagy plays a dual role in CSCs by preserving their drug resistance and supporting the maintenance of their stemness, as well as tumor proliferation. Publications indicate that mitophagy bolsters both the stem-like properties and chemotherapeutic resilience of CSCs in oral squamous cell carcinoma [29]. Furthermore, curtailing Drp1 function by inhibiting COX-2 has been demonstrated to diminish stem-like qualities, which in turn makes nasopharyngeal carcinoma cells more receptive to the effects of 5-fluorouracil [28]. Hence, within the realm of oncological treatment, pinpointing biomarkers related to mitophagy might steer towards therapies that are more precise, efficacious, and lower in toxicity.

In our study, we initially explored the expression levels and prognostic value of mitophagy-related genes at the pan-cancer level. Subsequently, we integrated multi-omics data to elucidate the molecular characteristics, biological functions, infiltration levels in the tumor microenvironment, and clinical significance of different types of mitophagy alterations in HNSCC. Furthermore, we developed and validated a prognostic tool named Mitophagy Subgroup Risk Score (MSRS), aimed at predicting the prognosis and immune response of HNSCC patients, and applied it at the single-cell level to explore intercellular communication. Concurrently, laboratory experiments validated the biological function of SLC26A9, one of the genes in MSRS.

MATERIALS AND METHODS

Collection and management of data

The gene expression profiles and clinical information of HNSCC were downloaded from the UCSC Xena

database [30]. Copy number variation data for head and neck squamous cell carcinoma were downloaded from the TCGA website using the R-package TCGAbiolinks. Tumor immune cycle scores were downloaded from the TIMER2.0 database. The specific transcription factors for HNSCC (Supplementary Table 1) were downloaded from the HumanTFDB (http://bioinfo.life.hust.edu.cn/HumanTFDB) database.

Categorization of mitophagy subtypes in HNSCC

A total of 29 Mitophagy-Related Genes (MRGs) (Supplementary Table 2) were retrieved from databases such as Reactome, CPDB, KEGG, and MSigDB [31–34]. Using R package 'corrplot', we evaluated correlations among these genes. HNSCC patients were classified into mitophagy subgroups (k=3) using the "ConsensusClusterPlus" R package [35]. Subsequently, differential expression genes between subtypes were analyzed using the "limma" R package.

Pathway enrichment in subgroups

Pathway enrichment was performed using the GSVA method through the GSVA R package, with pathway enrichment data sourced from gmt files in the MSigDB [31] and ConsensusPathDB [33] databases.

Analysis of the tumor microenvironment (TME)

We assessed the immune cell composition in the TME of various subgroups using algorithms such as TIMER, CIBERSORT, QUANTISEQ, MCPCOUNTER, XCELL, and EPIC. Additionally, ssGSVA was applied to validate differences in immune infiltration across HNSCC subgroups [36–39]. The infiltration levels based on immune and stromal scores in HNSCC were calculated using the "ESTIMATE" R package.

Mutation profile analysis in subgroups

We used the "Maftools" R package to compare mutation patterns across different subgroups [40]. Functions within "Maftools" were used to calculate mutation spectra for different mitophagy subgroups and to explore drug-gene interactions and carcinogenic pathways [41]. Additionally, somatic copy number alterations were analyzed using GISTIC 2.0 [42].

Evaluation of chemotherapy response disparities among subgroups

Based on the GDSC database [43], we used the "oncoPredict" R package [44] to assess differences in drug sensitivity among subgroups. Furthermore, the CellMiner [45] and CCLE [46] databases were used to analyze the correlation between mitophagy-related genes and drug sensitivity in HNSCC cell lines.

Machine learning algorithms

To construct the Mitophagy Subgroup Risk Score (MSRS), we integrated ten different machine learning algorithms, including RSF, Enet, Lasso, Stepwise Cox, Ridge, CoxBoost, plsRcox, SuperPC, GBM, and survival SVM. We applied 94 different combinations of these algorithms to identify the one with the highest average concordance index (C-index) across multiple cohorts. The "timeROC" R package was used to calculate the Area Under the Curve (AUC) to verify the accuracy of the MSRS. Additionally, the independent predictive capability of the MSRS was confirmed using Cox regression analysis in the "survival" R package.

Cell–cell communication analysis

We used GSE181919 dataset to explore the role of mitophagy genes at the single-cell level. R package "Seurat" was used to perform dimension reduction and clustering analysis, and the annotation of cell cluster was obtained by R package "SingleR". We employed the 'CellPhoneDB' package [47] to explore communication at the cellular level between immune and HNSC cells, concentrating on the identification of distinct ligand-receptor pairs.

Immunotherapy efficacy prediction

We used the Tumor Immune Dysfunction and Exclusion (TIDE) algorithms [48, 49] to predict responses to immune checkpoint blockade (ICB) therapy. The patient cohorts for this immunotherapy study were derived from the TIGER database [50], which includes the GSE91061 (melanoma) and phs000452 (melanoma) datasets.

Cultivation of cell lines

HNSC cell lines including SCC15 and HN30 were obtained from the public laboratory of Tianjin Medical University Cancer Institute and Hospital. For their cultivation, we used DMEM enriched with 10% FBS and 1% penicillin-streptomycin. The incubation conditions for these cell lines were carefully controlled, while the environment was maintained at constant temperature of 37° C with an atmosphere of 5% CO_2, ensuring optimal growth conditions and allowing for accurate and reliable experimental results.

siRNA transfection

For transfection studies, SCC15 and HN30 cell lines were seeded into 6-well plates. According to the

protocol provided by the supplier, transfection was carried out using si-SLC26A9-1 (sequence 5'- CAGCC AAGAUCAAAGCUGUGGUGUU -3'), si-SLC26A9-2 (sequence 5'- GGGCUUCAUGCAGUUUGGCUUUG UG -3'), and a non-targeting siRNA control (sequence 5'- CAGAAAGCUAAGAUCUGGGUCCGUU-3') with Hieff Trans® Liposomal Transfection Reagent (Yeasen, China). The knockdown efficiency was verified by Western blot 48 hours post-transfection.

Cell viability assay

Cells were collected through a process of digestion followed by centrifugation. After counting the cells, they were seeded into 96-well plates at a density of 2,500 cells per well. To assess cell viability, we utilized a Cell Counting Kit-8 (ApexBio, USA), conducting measurements at intervals of 0, 24, 48, and 72 hours according to the instructions provided with the kit. This methodical approach allowed us to accurately monitor the health and proliferation of the cells over time.

Cell lysis and western blotting

Cell lysis for protein extraction was performed at cold temperatures using a lysis buffer containing phosphatase and protease inhibitors. Protein levels were quantified with the SDS. The proteins were separated by 4-12% SDS-PAGE, transferred to PVDF membranes, blocked, and incubated with primary and secondary antibodies sequentially. Detection of the target proteins was achieved using a chemiluminescence reagent. The primary antibodies applied were anti-SLC26A9 (ABclonal, A18530) and anti-beta-actin (Santa, sc-8432).

Transwell assays and wound healing assays

SCC15 and HN30 cells, post transfection with either si-SLC26A9-1, si-SLC26A9-2, or si-NC, were harvested, washed with PBS, and subsequently resuspended in DMEM medium. These cells were then placed into the upper chamber of a 24-well plate which contains an insert with 8 μm pore size. In the lower chamber, 700 μL of DMEM containing 10% FBS was added. Following a period of 24 hours, cells remaining on the upper surface were wiped off, and those adhered to the lower surface were fixed with 4% paraformaldehyde (PFA) and stained with crystal violet for further image acquisition and analysis.

Wound healing assay

SCC15 and HN30 cells transfected with siRNA were cultured in 6-well plates to near confluence. Subsequently, a sterile pipette tip was used to create scratches through the monolayer. Photographs were taken immediately (0 hours) and at 48 hours after the scratch was made. The healing progress was quantified using the ImageJ software.

Colony formation assay

To assess the colony formation capacity of the cells, we carefully seeded between 800 to 1000 cells in each well of 6-well plates. These were then incubated at a consistent temperature of 37° C for a duration of 10 to 14 days to allow sufficient time for colony development. Following the incubation period, we fixed the colonies using methanol for 15 to 30 minutes, ensuring their preservation for analysis. This step was followed by staining with 0.1% crystal violet for 15 minutes to highlight the colonies for easier counting. The final step involved meticulously counting the colonies, providing a clear measure of the cells' ability to proliferate and form colonies under the given conditions.

EdU assay

After transfection process the cells were plated into 24-well plates ($5 * 10^4$ cells) and cultured overnight in a 37° C incubator. Following the protocol provided by the BeyoClick EdU Cell Proliferation Kit with Alexa Fluor 488, EdU detection was performed, EdU-positive cells were stained with Azide 488 and Hoechst 33342 to differentiate them from non-proliferative cells. We captured images from three randomly selected fields of view under a microscope to ensure a representative sampling. The percentage of EdU-positive cells was calculated by the following formula: EdU-positive rate = EdU-positive cell count/(EdU-positive cell count + EdU negative cell count) × 100%.

Statistical analysis

Experimental results are presented as mean ± standard deviation. We employed the chi-squared test to explore differences in categorical variables, including clinical characteristics, among various subgroups to identify significant variations P-value of less than 0.05 was considered to indicate statistical significance. The Benjamini-Hochberg (BH) method was applied to calculate adjusted P-values for multiple testing corrections. All data processing, statistical analyses, and the generation of graphical representations were conducted using R software (version 4.1.3), ensuring rigorous and comprehensive analysis.

Availability of data and materials

The open-access datasets are available through the following URL: GSE41613, GSE42743, GSE65858,

and GSE181919 (https://www.ncbi.nlm.nih.gov/geo/) and the Cancer Genome Atlas (TCGA) HNSC project (http://xena.ucsc.edu/).

RESULTS

The role of mitophagy in cancers and its impact on patient survival

Figure 1 illustrates the sequential steps of our research process. We investigated the complex regulation of mitophagy in various cancer types by assessing the expression levels of mitophagy-related mRNAs in diverse cancer types. Our findings indicate that the expression levels of CSNK2B, MTERF3, and PGAM5 are elevated in multiple cancers, while the expression levels of PINK1 and PRKN are reduced in several cancers (Supplementary Figure 1A). We used Spearman (upper right) and Pearson (lower left) correlation analysis to study the relationship between Mitophagy-Related Genes (MRGs) in the TCGA-HNSCC dataset, identifying significant associations between RPS27A and TOMM22, TOMM7, UBA52 (Supplementary Figure 1B). Furthermore, our study revealed the connection between gene expression profiles and patient prognosis (Supplementary Figure 1C), finding that most MRGs act as risk factors in HNSC, LIHC, KICH, LUAD, LUSC, BRCA, while TOMM6 serves as a protective factor in THYM, OV, DLBC, and PINK1 as a protective factor in KIRC, KIRP, ACC.

Copy number and mutation events of mitophagy regulators in cancers

To further explore the reasons for changes in mitophagy-related genes, we validated copy number variations (CNV) in cancer and observed a significant positive correlation between CNV and mRNA expression (Figure 2A). As shown in Figure 2B, genes such as MTERF3, TOMM7, CSNK2A1, SRC, TOMM20, and MAP1LC3A commonly exhibit heterozygous amplification in tumors, whereas UBB, TOMM22, MAP1LC3B, and PRKN mainly show heterozygous deletion. However, homozygous amplifications and deletions were found to be infrequent (Figure 2C). Figure 2D displays the genomic locations of CNVs in mitophagy-related genes. Notably, in HNSCC, genes such as TOMM7, TOMM70, MTERF3, and MFN1 have a higher frequency of CNV amplification, while SQSTM1, VDAC1, and ATG12 have a higher frequency of CNV deletion (Figure 2E). Furthermore, we delved into the mutation status of mitophagy-related genes and found that these genes have a higher mutation frequency in UCEC, COAD, SKCM, STAD, BLCA, LUSC, and LUAD, but mutations are rare in PCPG, MESO, and KICH (Figure 2F).

Defining three subgroups within HNSCC based on mitophagy regulator expression

We employed an unsupervised clustering algorithm to divide TCGA-HNSCC samples into three distinct molecular subgroups based on the expression profiles of mitophagy-related genes (Figure 3A, 3B). Patients in Cluster A exhibited a significantly enhanced survival advantage compared to those in the other two clusters (Figure 3C). Additionally, within Clusters B and C, a specific subset of mitophagy related genes shown not significantly higher expression levels. TOMM20, TOMM22, CSNK2B, UBA52, RPS27A, TOMM7 were less expressed in Cluster A, while in Cluster B, the expression levels of ULK1, CSNK2A2, MAP1LC3B, UBC, MFN2, PINK1 were lower. However, the expression of mitophagy-related genes was higher in Cluster C (Figure 3D).

Enrichment analysis of functional pathways in varied patterns of mitophagy alterations

We employed Gene Set Variation Analysis (GSVA) to assess metabolic pathway signatures. Cluster A was characterized by metabolic dormancy, showcasing downregulation in pathways such as glucose, amino acid, nucleotide, and RNA metabolisms, the TCA cycle, and tyrosine metabolism. Conversely, Clusters B and C demonstrated metabolic exuberance with these signatures predominantly active, hinting at an augmented metabolic state (Supplementary Figure 2A). Furthermore, GSVA revealed a consistent enrichment of the hypoxia signature in Cluster B (Supplementary Figure 2B), a condition known to hinder cancer immunotherapy effectiveness due to reduced oxygen levels in tumors [51–53]. Addressing hypoxia might thus potentiate immunotherapeutic outcomes for patients in Cluster B. Additionally, an attenuated exosomal signature in Cluster B implicates a potential interplay between mitophagy and exosome dynamics (Supplementary Figure 2B).

To further our transcriptomic investigation, we harnessed RTNduals [54], an R-based analytical package, to decipher transcription factor regulons specific to mitophagy subtypes, sourced from the HumanTFDB. Notably, ZFP36L1 activity was minimal in Cluster B, suggesting a dampened cell cycle mechanism in this subgroup (Supplementary Figure 2C). Given recent insights linking ZFP36L1 [55] to immune infiltration in tumor microenvironments, these findings suggest that alterations in mitophagy may regulate crucial biological functions.

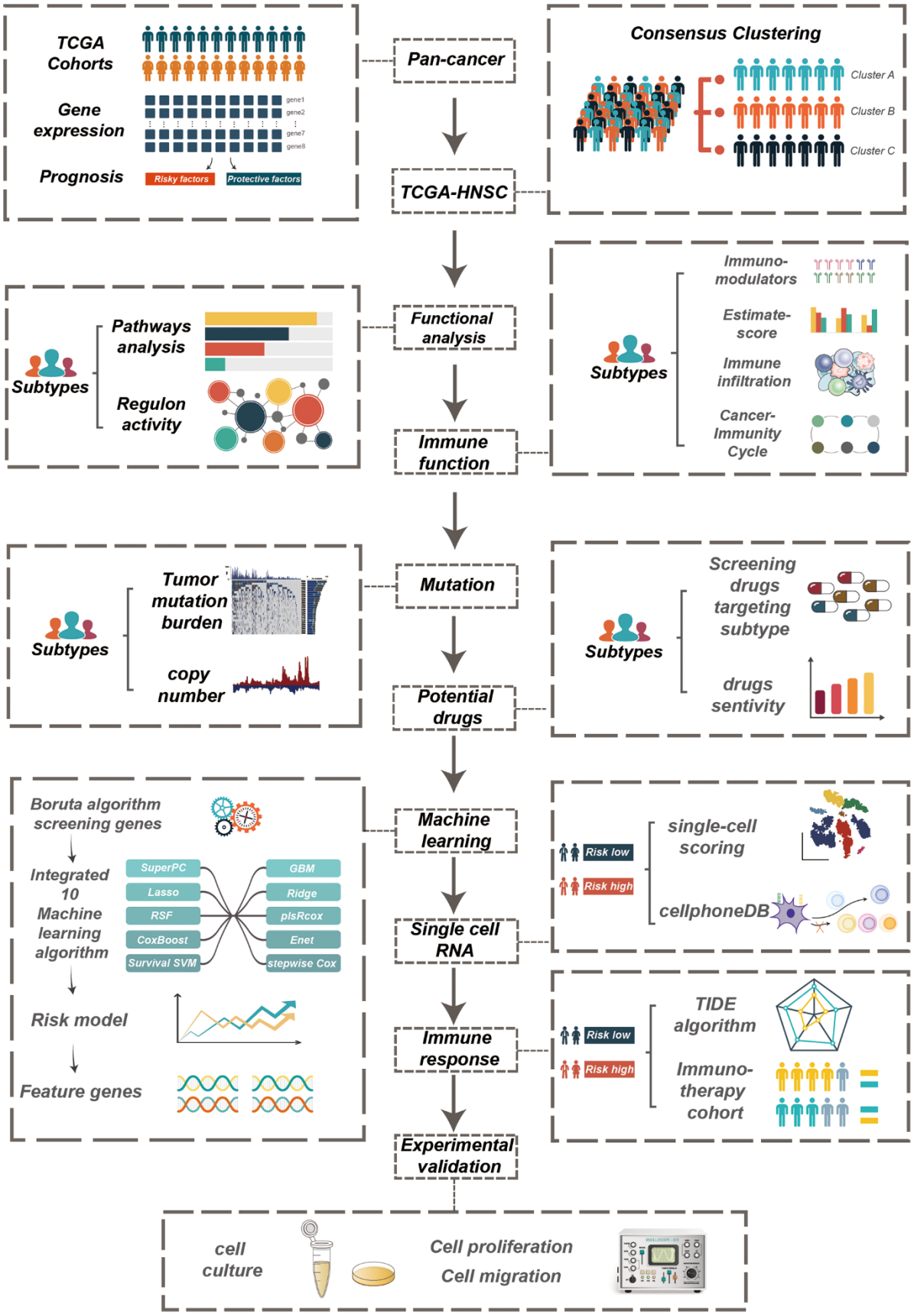

Figure 1. The workflow of the study.

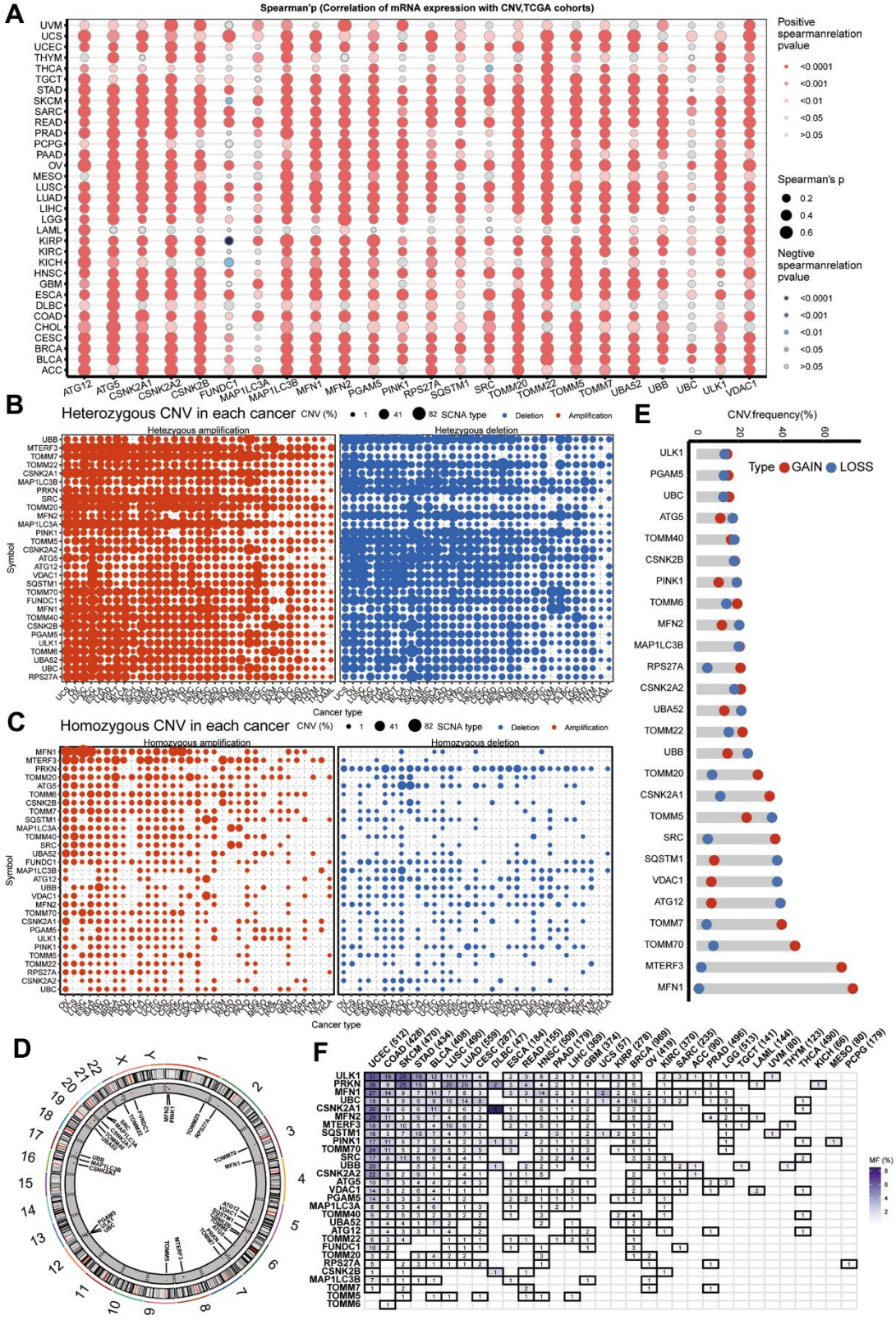

Figure 2. CNV and sequence alteration contribute to abnormal mitophagy genes Levels. (**A**) CNV strongly correlates to gene expression of mitophagy regulators in pan-cancer using spearman analysis. (**B**, **C**) Heterozygous and homozygous amplification/deletion of mitophagy regulators in pan-cancer. Amplification, red; Deletion, blue. (**D**) The location of CNV of mitophagy regulators on 23 chromosomes. (**E**) CNV of mitophagy regulators in TCGA-HNSC dataset. CNV loss, blue; CNV gain, red. (**F**) Mutation frequency of mitophagy regulators in pan-cancer.

Assessing distinct immune profiles across mitophagy subgroups

To compare immune activity among various subgroups, we evaluated immune process enrichment scores across different subgroups using Gene Set Variation Analysis (GSVA). Notably, Cluster B was marked by a pronounced decrease in pathways related to chemokines, chemokine receptors, immune inhibitors, and immune stimulators (Supplementary Figure 3A). Further analysis

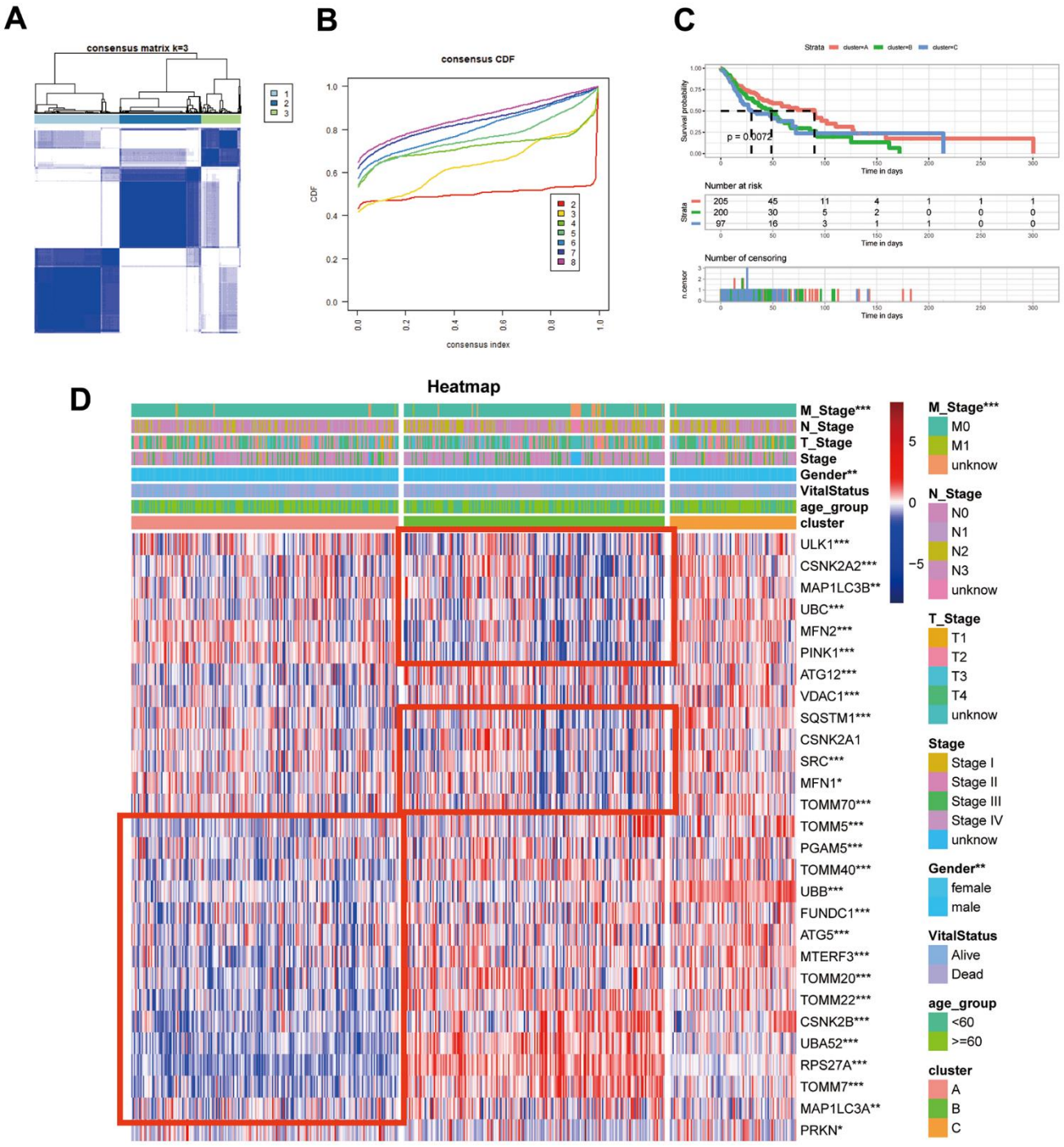

Figure 3. Identification of mitophagy subtypes of HNSCC. (**A**) Consensus matrix of samples in TCGA-HNSC for k=3. (**B**) The cumulative distribution function curves for k = 2 to 8. (**C**) Kaplan-Meier survival analysis for overall survival of the three subtypes in TCGA-HNSC dataset. (**D**) The expression profiles of the mitophagy regulators in three subtypes and normal kidney samples. Statistical significance denoted as ****$p < 0.0001$, ***$p < 0.001$, **$p < 0.01$, *$p < 0.05$.

of the tumor microenvironment (TME) cell composition revealed a substantial reduction in immune cell infiltration in Cluster B compared to Clusters A and C, as shown in Figure 4A. This suggests that Cluster B might represent an 'immune desert' phenotype with notably reduced immune engagement.

This observation is in line with survival analyses, where Cluster B patients had poorer outcomes compared to those in Cluster A. Our focus then turned to dissecting the anti-cancer immune cycle, which involves multiple critical steps. In Cluster B, there was a notable decrease in key phases of this cycle, including Cancer cell antigens are released (Step 1), and immune cells such as CD4 and CD8 T cells, macrophages, NK cells, Th1, Th2, and Th22 cells are mobilized (Step 4), along with their infiltration into the tumor (Step 5), as depicted in Figure 4B.

Tumor genomic alterations and CNV profiles in three mitophagy subgroups

Among the three defined groups, we analyzed the distribution of tumor somatic mutations. Supplementary Figure 4A–4C show the top 25 most frequently mutated genes, indicating a high mutation burden across all subgroups. Additionally, we assessed druggable targets based on these mutations, using the DGIdb and the maftools package to investigate drug-gene interactions. Potential therapeutic targets related to the three mitophagy modification patterns were categorized into 19, 18, and 20 groups, which included targets within clinically relevant, druggable genome, kinase, and histone modification categories, as detailed in Supplementary Figure 4D–4F. Employing the R package maftools, we examined less common genetic changes in cancer pathways including RTK-RAS, Hippo, WNT, TP53, and the Cell Cycle. In Cluster A, the NRF2, TP53, and TGF-Beta pathways were most affected, while Cluster B showed a pronounced impact on the NRF2 and TGF-Beta pathways. Cluster C affected the NRF2 and RTK-RAS pathways most significantly, as shown in Supplementary Figure 4G–4I.

In our comparative assessment of Copy Number Variation (CNV) among the clusters, Cluster B showed the highest rate of CNV, with Clusters C and A following closely, as demonstrated in Figure 5A. This observation is supported by similar trends in the percentage of gain/loss and GISTIC scores for amplification and deletion regions on chromosomes analyzed using GISTIC 2.0, as depicted in Figure 5B, 5C. These insights suggest that diverse CNVs play a role in defining the distinct mitophagy-related tumor subtypes.

Chemotherapeutic response variations among mitophagy subgroups

We conducted a comparative analysis of drug sensitivity using IC_{50} values obtained from the GDSC database. Our analysis predicted enhanced sensitivity to palbociclib for patients categorized within Cluster B. It was found that gefitinib, navitoclax, and dasatinib were more potent for patients in Cluster A, while those in Cluster C were more responsive to temozolomide, cisplatin, and tamoxifen, as indicated in Supplementary Figure 5.

Subsequently, we sought to identify treatments that counteract cancer-driving processes. We examined the relationship between mitophagy gene expression and drug sensitivity using data from the CellMiner database. We found that the expression of PINK1 inversely correlates with the IC_{50} values for AFP464, palbociclib, and denileukin diftitox (Supplementary Figure 6), implying that patients with higher PINK1 expression may benefit more from these drugs. Additionally, Econazole nitrate and Crizotinib appeared to be more effective in individuals with lower expression of RPS27A and TOMM7, respectively.

Construction of the mitophagy subgroup risk score (MSRS) by integrated machine learning

By employing the Limma algorithm, the computation of unique genes for the three subcategories and the assessment of overlaps were conducted, leading to the discovery of a grand total of 468 genes linked to mitophagy subtypes (Supplementary Table 3). Univariate Cox regression analysis (Supplementary Table 4) revealed 194 genes that exhibited a significant association with overall survival. Out of the 194 prognostic genes, the bootstrap technique identified 19 genes that remained stable even after resampling the samples and were also present in the validation datasets (Supplementary Table 5). Furthermore, we employed the Boruta algorithm and narrowed down the selected genes to a group of 10 genes that were confirmed to have greater importance in terms of recurrence (Supplementary Figure 7), as illustrated. Based on their inferred degree of importance, the Boruta algorithm ranked 10 genes, identified as Figure 6A.

We employed our machine learning algorithm to scrutinize these 10 genes and develop a predictive model. Utilizing 94 forecasting models, we examined the TCGA dataset and calculated the concordance index (C-index) for three validation datasets. Ultimately, the integration of the SuperPC algorithms yielded the most effective prototype, achieving an average C-index of 0.619 across all validation datasets, as illustrated in

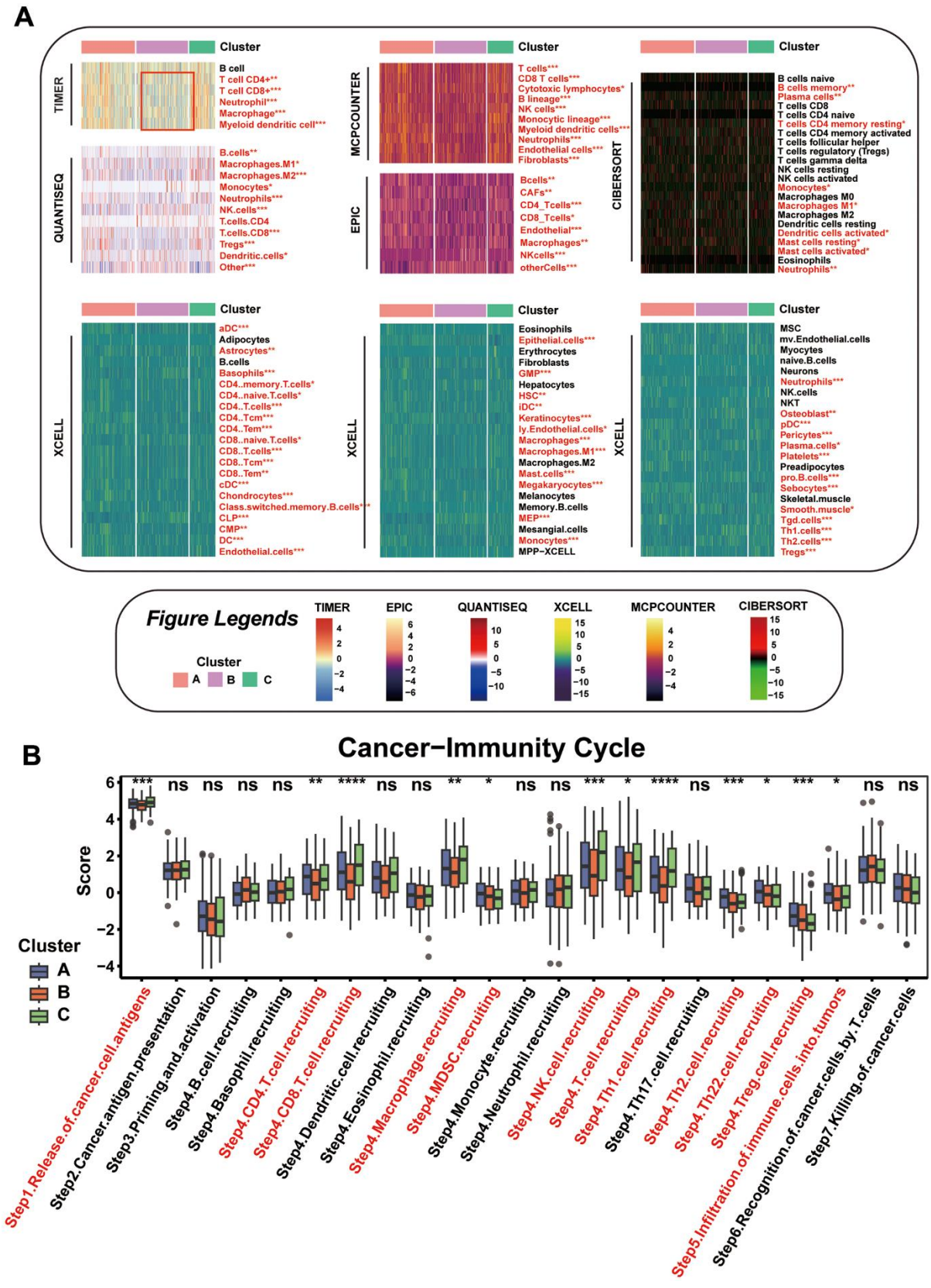

Figure 4. Comparison of the Specific Immune Infiltration Landscape among Three Subgroups. (**A**) Heatmap of immune cell infiltration among the subtypes. (**B**) Boxplot of cancer immunity cycle in three mitophagy modification subtypes. Statistical significance denoted as ****$p < 0.0001$, ***$p < 0.001$, **$p < 0.01$, *$p < 0.05$.

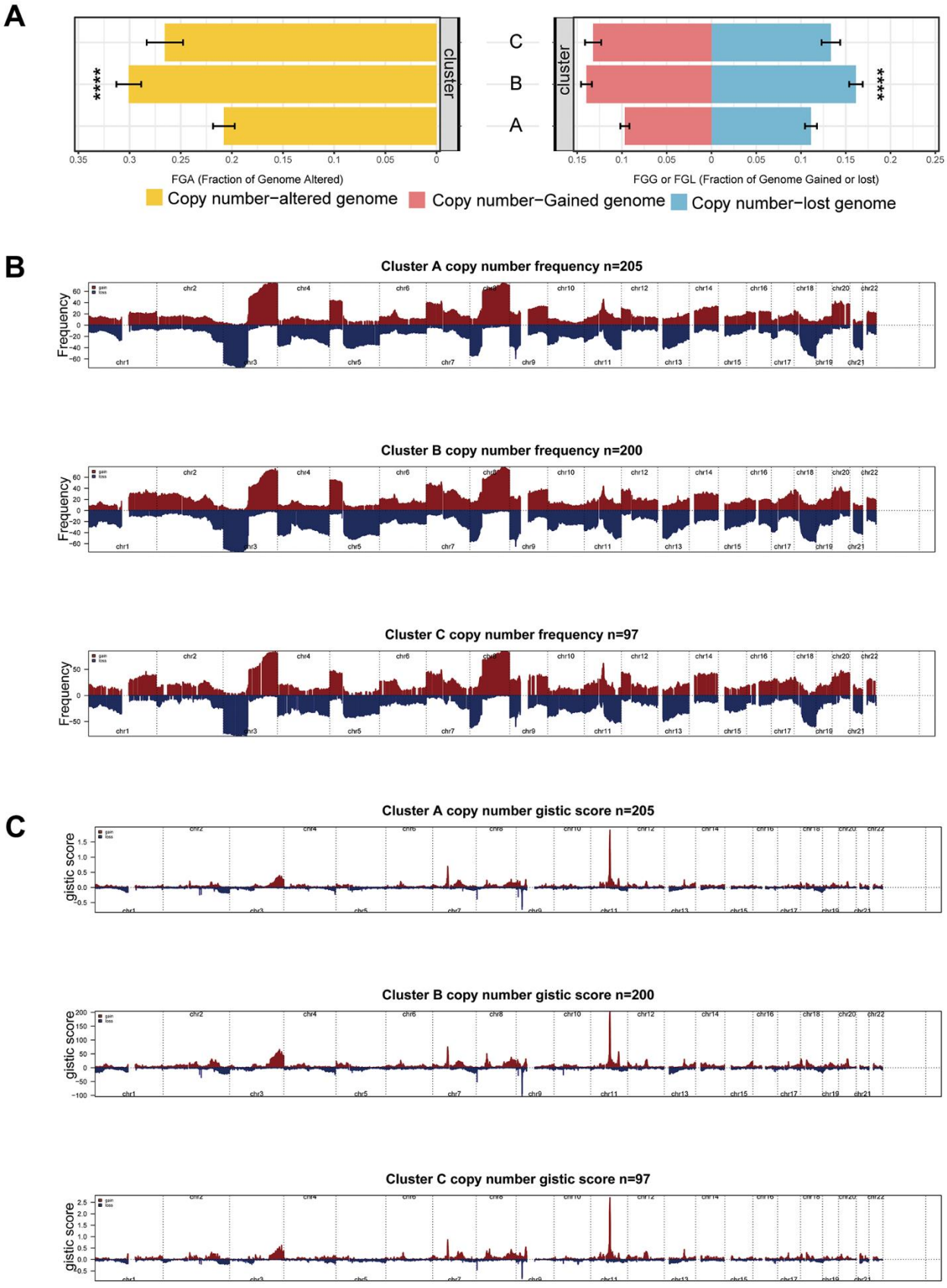

Figure 5. CNV differences among subgroups. (**A**) CNV rate among subgroups. (**B**, **C**) Differences of gain/loss percentage (**B**) and GISTIC score (**C**) in Cluster A, B, and C. Statistical significance denoted as ****$p < 0.0001$, ***$p < 0.001$, **$p < 0.01$, *$p < 0.05$.

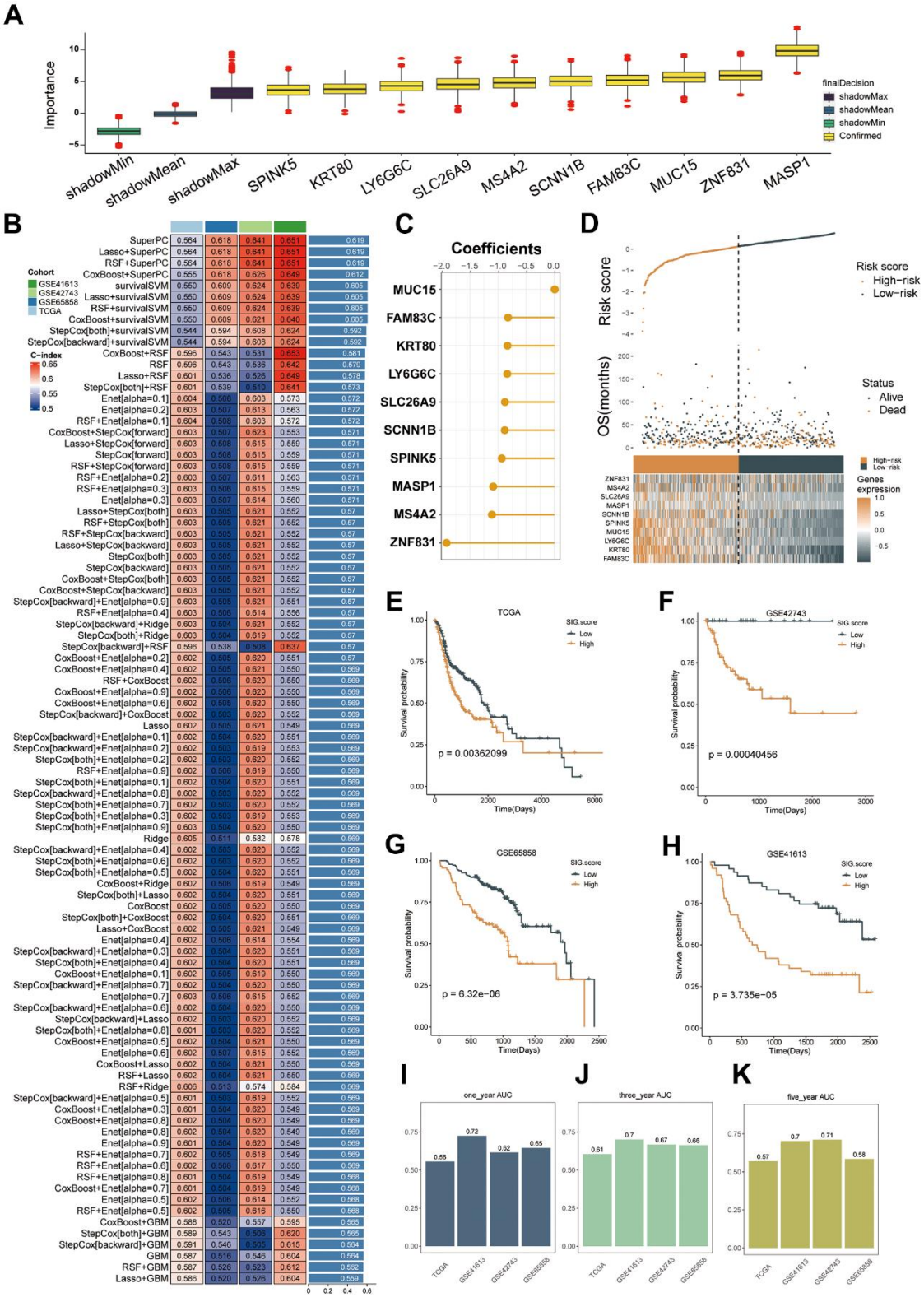

Figure 6. Machine learning-based gene signatures based on mitophagy subgroups. (**A**) The Boruta algorithm identified 10 mitophagy-related genes. Yellow represents confirmed features while other colors denote shadow attributes. The corresponding boxplots compared the concordance index (C-index) values. (**B**) Machine learning was used to build 93 different models, and their C-indices were tested in each verification set. (**C**) The coefficients of ten genes calculated by SuperPC. (**D**) Statistical analysis of the risk scores and survival status of ten genes as well as their expression characteristics in TCGA. (**E**–**H**) Prognoses of patients in the TCGA (**E**), GSE42743 (**F**), GSE65858 (**G**), and GSE41613 (**H**) sets. (**I**–**K**) Predicting patient survival at 1, 3, and 5 years using the MSRS.

Figure 6B. The SuperPC algorithm revealed 10 crucial genes for determining the risk score, as depicted in Figure 6C. The calculation of MSRS involved the evaluation of the expression levels of these 10 genes and their respective regression coefficients for every individual within the mitophagy subgroup.

As Figure 6D–6H, there was a correlation between an escalation in the MSRS, a decrease in the overall survival (OS), and an elevation in the mortality rates. Patients were categorized into high-risk and low-risk groups based on the median MSRS value. Consistently, the TCGA training dataset and the three validation datasets showed that the high-risk group had significantly worse survival outcomes than the low-risk group, as depicted in Figure 6E–6H. In TCGA-HNSC, the ROC analysis verified that the MSRS has a robust ability to discriminate, as evidenced by AUC values of 0.56, 0.61, and 0.57 for one-, three-, and five-year survival, respectively. displays the AUCs for GSE41613 as 0.72, 0.7, and 0.7; for GSE42743 as 0.62, 0.67, and 0.71; and for GSE65858 as 0.65, 0.66, and 0.58.

Interactions between immune cells and HNSC cells that involve ligand–receptor pairs

To investigate the potential interaction between immune cells (T cells, B cells, etc.) and head and neck squamous cell carcinoma (HNSC) cells, we utilized single-cell RNA sequencing (scRNA-seq) to analyze their collaboration. Initially, we calculated risk scores for various cell types and discovered that epithelial cells exhibited the lowest risk score, as illustrated in Supplementary Figure 8A. Supplementary Figure 8B shows that risk scores were higher in tumor tissue-associated cells than in normal tissues.

Afterwards, we conducted a thorough analysis of the associations between high-risk epithelial cells (Riskhighepi) and low-risk epithelial cells (Risklowepi) along with other cellular components using CellphoneDB in combination with scRNA-seq data. As shown in Supplementary Figure 8C, when acting as a receptor or ligand, Riskhighepi has a significantly greater number of ligand-receptor pairs in interactions with other cells than Risklowepi. Supplementary Figure 8D illustrates the interaction intensity between Riskhighepi and other cell types, showing notably stronger interactions with endothelial cells, fibroblasts, and smooth muscle cells. Upon contrasting the communicative signals with Riskhighepi, we identified that the signaling pathway showing a robust interaction between Risklowepi and Smooth muscle cells involved COL17A1_a2b1_ complex, COL17A1_a10b1_complex, and COL17A1_ a1b1_complex (Supplementary Figure 8E). The pathway connecting Risklowepi and Fibroblasts included COL17A1_a1b1_complex, COL17A1_a11b1_complex, and MIF_TNFRSF14 (Supplementary Figure 8F), and the interaction between Risklowepi and endothelial cells featured MIF_TNFRSF10D, MIF_TNFRSF14, and COL17A1_a1b1_complex (Supplementary Figure 8G). Furthermore, we noticed that the signal indicating the most prominent connection between Risklowepi and other immune cells was linked to either COL17A1 or MIF (Supplementary Table 6).

MSRS's ability to predict ICB efficacy

To validate the immunotherapy predictive performance of the Mitophagy Subgroup Risk Score (MSRS), we assessed it using the TIDE website. We found that in the group with lower MSRS, the TIDE scores and exclusion scores were lower, while the dysfunction scores were higher (Supplementary Figure 9A–9C). Furthermore, individuals with decreased MSRS exhibited a decline in the infiltration of cancer-associated fibroblasts (CAFs), as illustrated in Supplementary Figure 9D–9G. In summary, these findings suggest that people with decreased MSRS scores exhibit increased responsiveness to immuno-therapy.

In the GSE91061 cohort, a higher proportion of patients with lower MSRS had a response to immunotherapy (Supplementary Figure 9H). The findings from the GSE91061 and phs000452 immunotherapy cohorts also supported the idea that patients who had a low MSRS and received immunotherapy had a better prognosis than those with a high MSRS, as shown in Supplementary Figure 9I, 9J. The potential of the MSRS as a predictive indicator for the effectiveness of immunotherapy in these specific patient cohorts is emphasized by this observation.

SLC26A9 is associated with tumor suppression in HNSC

Through laboratory experiments, we explored the biological function of SLC26A9, which is one of the genes in the Mitophagy Subgroup Risk Score (MSRS). Supplementary Figure 10 demonstrates that SLC26A9 is a protective factor in the prognosis of HNSCC. During our research, we utilized a collection of siRNAs to inhibit the expression of SLC26A9 in SCC15 and HN30 cell lines. After 48 hours of transfection, western blot analysis confirmed the successful knockdown of SLC26A9 (Figure 7A).

Afterwards, Figure 7B shows that the decrease in SLC26A9 resulted in improved cell viability. The 5-ethynyl-2'-deoxyuridine (EdU) incorporation assay revealed enhanced cell growth in both SCC15 and

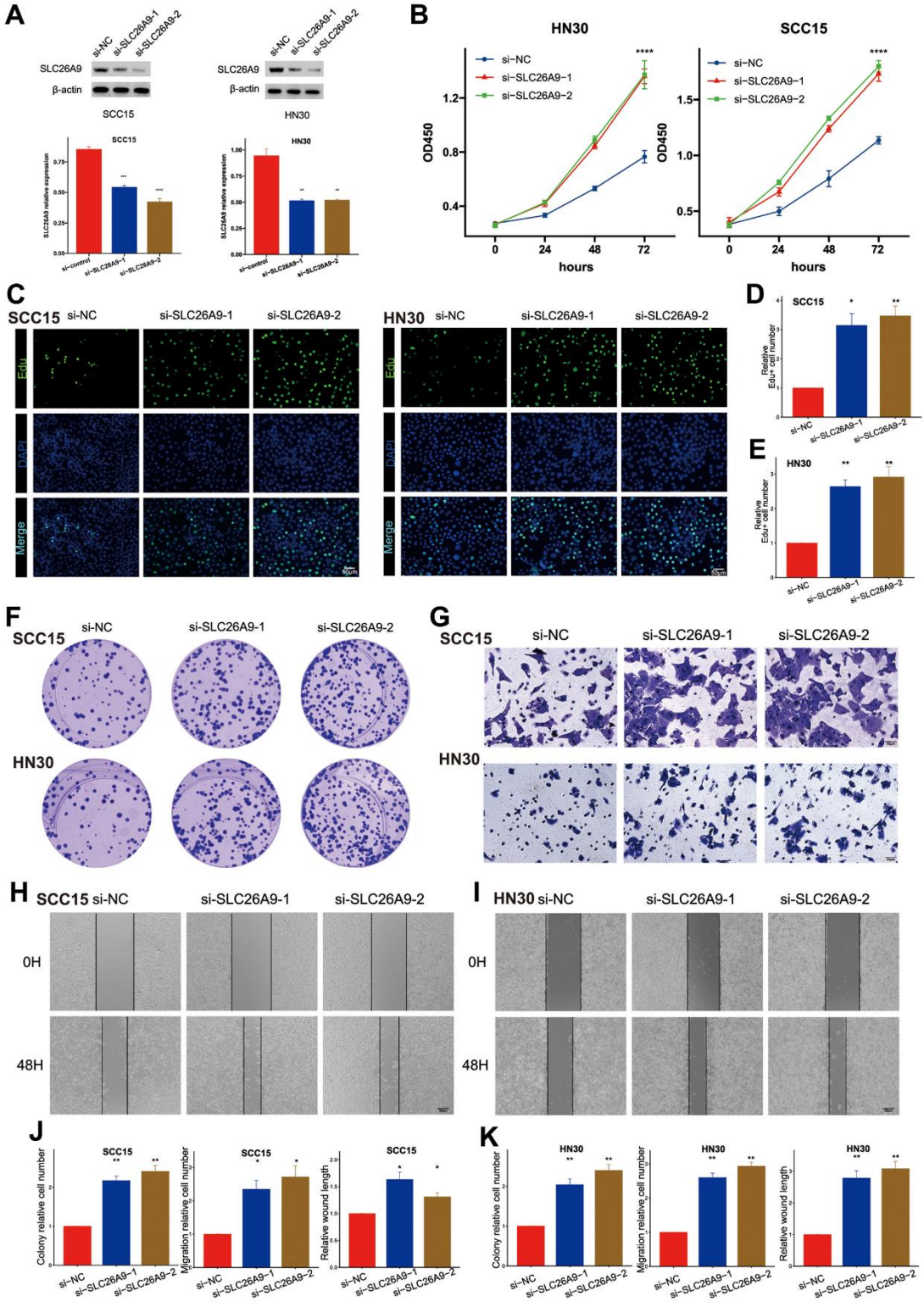

Figure 7. Knockdown of SLC26A9 promoted the proliferation and migration of HNSC cells. (**A**) SLC26A9 siRNA transfection levels analyzed via Western Blot. (**B**) CCK8 assay assessing cell viability in SCC15 and HN30 cells with reduced SLC26A9 expression. (**C**) EdU assay evaluating cell proliferation post SLC26A9 knockdown in SCC15 and HN30 cells. (**D**, **E**) Quantitative analysis of EdU-positive cell rates in SCC15 (**D**) and HN30 (**E**) cells. (**F**) Notable reduction in clone numbers in SCC15 and HN30 cells following SLC26A9 knockdown. (**G**) Transwell assay measuring migration capability of SCC15 and HN30 cells with decreased SLC26A9 expression. (**H**, **I**) Cell scratch assay examining proliferation in SCC15 (**H**) and HN30 (**I**) cells post SLC26A9 reduction. (**J**, **K**) Quantitative summary of clone numbers, migration rates in transwell assay, and wound healing rates in SCC15 (**J**) and HN30 (**K**) cells.

HN30 cell lines upon the observation of SLC26A9 inhibition. Moreover, a rise in the quantity of colonies was observed in the cell lines when SLC26A9 was diminished, as depicted in Figure 7C–7E. Moreover, the migratory capabilities of SCC15 and HN30 cells were notably enhanced following SLC26A9 knockdown, as evidenced by transwell and wound healing assays (Figure 7G–7J). The overall results suggest that SLC26A9 inhibits the proliferation and migration of HNSC cells, highlighting its therapeutic potential as a target for addressing this type of cancer.

DISCUSSION

Head and neck squamous cell carcinomas exhibit considerable heterogeneity. There is a critical demand for precise diagnostic tools and reliable prognostic indicators. Targeting mitophagy has gained prominence as a pivotal strategy in oncology, given its vital role in cellular survival and tumor growth. The progression of tumors has been associated with key players in the mitophagy pathway such as PINK1 [56], Parkin [57], BNIP3 [58], and FUNDC1 [59]. Therapeutic benefits have been observed by disrupting the activity of these proteins in cancer therapies. Additionally, a focus on mitophagy has often led to an increased susceptibility of cancer cells to pharmacological treatments. Inhibiting mitophagy has been noted to elevate chemosensitivity in tumor cells, reducing their ability to resist drug interventions, particularly through the action of PINK1 [60]. Moreover, blocking FUNDC1 has been noted to increase the responsiveness of cervical cancer cells to both cisplatin and radiation therapy. It has been documented that salinomycin can initiate mitophagy, which serves as a protective mechanism in tumor cells. A reduction in ATG5 has also been shown to promote apoptosis in malignant and cancer stem cells [61]. Additionally, the compound liensinine, a type of isoquinoline alkaloid, not only impedes mitophagy but also heightens the susceptibility of cancer cells to a range of anti-cancer drugs. Liensinine impedes the merging of autophagosomes with lysosomes, causing an accumulation of mitophagosomes, which consequently induces mitochondrial division through DNM1L and leads to cell death [62]. There is growing evidence that mitophagy is integrally involved in glycolysis [63], tumor development [64], activation of inflammasomes [65], and the preservation of stem cell characteristics [23, 66], via its regulatory interactions. While most research has concentrated on individual regulatory molecules, the collective impact of multiple mitophagy modulators on cancer attributes is not yet fully comprehended.

In our research, key mitophagy-related genes were scrutinized across various cancers, culminating in the discernment of three mitophagy-based classifications (Clusters A, B, and C) in individuals with HNSCC. We conducted an in-depth comparative analysis of these clusters, assessing them across multiple omics facets. This comprehensive approach resulted in the creation and validation of a prognostic tool, named MSRS, which effectively predicts patient outcomes in HNSCC.

The study exposed significant correlations between mitophagy-related genes across different cancers, suggesting a shared regulatory axis. Further scrutiny hinted that copy number variations and genetic aberrations could be driving the deregulation of mitophagy-related genes in oncogenesis. The research also unveiled distinctive clinical attributes within the three mitophagy patterns, highlighting how disruptions in mitophagy modulate the clinical trajectory of HNSCC sufferers. Notably, subjects in Cluster A manifested enhanced survival rates compared to those in Clusters B and C, which were linked with more advanced disease grades and stages.

Metabolic alteration is a hallmark of HNSCC, typifying its status as a malignant archetype [67, 68]. By conducting an enrichment analysis of transcriptomic variations, the current study identified strong links between metabolic pathways and distinct mitophagy subgroups. Metabolic functions appeared notably suppressed in Cluster A compared to Clusters B and C, pointing to metabolic intervention as a potential therapeutic avenue. Further scrutiny exposed distinct signaling dynamics within the cancer milieu among the clusters, with a marked suppression of the mitophagy signature in Cluster A. Intricate epigenetic regulatory mechanisms, involving complex modifications and interactions [69, 70], are known to initiate mitophagy, prompting our focus towards the epigenetic landscape as an actionable area. We also hypothesize that the group-specific functional disparities might be steered by key transcriptional regulators such as YBX1, TP53, ATF4, and NME2, meriting further investigation. These insights underscore the pivotal influence of mitophagy on diverse cell functions.

In head and neck squamous cell carcinoma (HNSCC), the tumor microenvironment (TME) is composed of a diverse mixture of neoplastic and assorted stromal cells, including endothelial cells, cancer-associated fibroblasts (CAFs), and components of the immune system. A prevalent feature of many HNSCC tumors is a marked immunosuppression within the TME [71, 72]. T lymphocytes and NK cells play vital roles in the TME, bolstering the host's anti-tumor defenses. In contrast, T regulatory cells, MDSCs, and M2 macrophages play a counteractive role, promoting tumor growth. A higher presence of CD8 T cells and NK cells [73, 74] in the

TME correlates with increased survival rates, while greater populations of MDSCs [75], neutrophils [76], and M2 macrophages [77] align with advanced HNSCC stages or adverse outcomes. Research indicates that mitochondrial autophagy in cancer significantly contributes to the infiltration of immune cells [65]. IL1B (interleukin 1 beta), pivotal components of the IL1 family, are associated with neutrophil migration, T cell differentiation and activation, NK cell engagement, and macrophage functions [78–80]. Growing research suggests that linear autophagy downregulates IL1B production through the regulation of NLRP3 [81–84]. IFNA and IFNB, are multifunctional cytokines enhancing antigen presentation, NK cell activities, and lymphocyte reactions [85]. The suppression of IFNA/IFNB synthesis by mitophagy was initially noted in ATG5-deficient cells, characterized by dysfunctional mitochondrial accumulation and elevated IFNA/IFNB generation [86]. Control of dysfunctional mitochondria associate mitophagy with other inflammatory cytokines, influencing immune cell infiltration. For instance, an increase in mtROS from autophagy deficiency leads to an overproduction of MIF (macrophage migration inhibitory factor) in human and mouse macrophages when stimulated by lipopolysaccharide. Besides impacting immune cell infiltration via pro-inflammatory cytokines, mitophagy can also directly exert effects on immune cells. Studies demonstrate a direct involvement of mitophagy in the development and differentiation of immune cells, such as T cells, NK cells, and macrophages. Additionally, the reduction of mitochondrial volume through autophagy is developmentally crucial for maintaining cell viability during the transformation of T cells from thymocytes to peripheral naïve T cells, as well as for the maturation of invariant NK T cells within the thymus [87, 88]. Significantly, the stage-specific control of BNIP3- and BNIP3L-mediated mitophagy is vital for the differentiation process of memory NK cells [89]. Additionally, IL10's suppression of mTOR activity triggers mitophagy while simultaneously slowing down glycolysis in lipopolysaccharide -stimulated macrophages, as noted in studies [90, 91]. Inhibiting mitophagy with 3-methyladenine encourages a shift towards inflammatory (M1) macrophages phenotypes, whereas promoting mitophagy with rapamycin hinders M1 polarization, favoring anti-inflammatory (M2) macrophages differentiation instead [92]. Building on these insights, we extended our research to examine the impact of mitophagy on immune functionality in head and neck squamous cell carcinoma.

Cluster B was characterized by a notably sparse infiltration of immune cells, indicative of immunosuppression and the 'cold tumor' phenotype, which is commonly resistant to immunotherapy. Research indicates that such tumors circumvent immune detection and hinder the proliferation and activation of T cells [93]. In Cluster B, the immune response was compromised by impediments in the release of cancer cell antigens and the subsequent T-cell engagement. Improving the immune response, particularly T-cell activation and patient survival, might be feasible by leveraging dendritic cell-mediated antigen presentation within the tumor milieu [94]. This aspect aligns with findings that individuals in Cluster B faced poorer prognoses compared to those in Cluster A. Further, our study explored examined the link between mitophagy and CNV alterations, with Cluster B showing a higher incidence of CNV changes, both deletions and amplifications, while Cluster A exhibited the least CNV frequency. The progression and complexity of HNSCC are thought to correlate with CNV patterns [95], and we postulate that genetic diversity may increase the likelihood of unpredictable clinical outcomes.

As previously noted, mitophagy can modulate the effectiveness of cancer treatments [81, 96]. Our analysis revealed differential drug response profiles among HNSCC patients categorized into the various clusters. Hence, our cluster categorizations could guide more precise drug deployment in therapeutic protocols. Additionally, our research also delves into potential treatment avenues for HNSCC, particularly for those in Cluster B, aiming to advance the knowledge of the molecular dynamics that govern the efficacy of these therapeutic interventions.

Our study aimed to enrich our understanding of HNSCC tumor biology by integrating patterns of mitophagy. To address individual variations, we amalgamated an extensive array of 94 machine learning techniques to forecast patient survival and their potential reaction to immunotherapy. Nevertheless, this research faces certain constraints. Primarily, our conclusions were drawn using thorough bioinformatic methods. There remains a need for experimental corroboration, especially in understanding the interplay of mitophagy regulators and the downstream pathways they influence. Additionally, despite observed variances in drug sensitivity across the subgroups, experimental confirmation is crucial. Furthermore, while we have validated our prognostic model, certain unavoidable confounders, like ethnicity and geographical location, may have introduced bias. For more robust conclusions, further independent datasets would be beneficial.

In closing, our research dissected the implications of mitophagy in HNSCC, distinguishing three mitophagy-related subgroups. We conducted an all-encompassing assessment of these subgroups' clinical profiles, biological roles, immune infiltration, genetic attributes,

and drug response patterns. Moreover, we constructed a solid mitophagy-based prognostic framework for forecasting HNSCC patient outcomes. The insights from our study offer a novel perspective on the mitophagy-HNSCC nexus, potentially aiding in clinical strategy formulation.

CONCLUSIONS

The MRGs were regarded as highly correlated with the prognosis of HNSCC and were recognized as exceptional prognosticators for HNSCC. Specific metabolic pathways and outcomes were linked to unique variations in mitophagy. Immune cell infiltration was more severe in subtypes that demonstrated increased levels of mitophagy. Moreover, there were differences in the way drugs responded among various subgroups. The Mitophagy Subgroup Risk Score (MSRS) is capable of effectively forecasting the immune treatment response and prognosis in patients with HNSCC. The Mitophagy Subgroup Risk Score (MSRS) gene SLC26A9 can inhibit HNSCC cell proliferation and migration. Examining the terrain of mitophagy alteration will increase understanding and further enrich the comprehension of HNSCC characterization. Additionally, it will provide guidance for future clinical decision-making.

AUTHOR CONTRIBUTIONS

Junzhi Liu and Huimin Li contributed equally. LJZ and LHM designed the research and performed the bioinformatics analysis and interpreted the results; LJZ and LHM performed the experiments, LJZ, LHM and DQP analyzed and interpreted the results; LJZ and LHM drafted the manuscript; LZ gave the final approval of the version to be published. All authors have read and agreed to the published version of the manuscript.

CONFLICTS OF INTEREST

The authors declare that they have no conflicts of interest to report regarding the present study.

FUNDING

This research received no external funding.

REFERENCES

1. Fitzmaurice C, Allen C, Barber RM, Barregard L, Bhutta ZA, Brenner H, Dicker DJ, Chimed-Orchir O, Dandona R, Dandona L, Fleming T, Forouzanfar MH, Hancock J, et al, and Global Burden of Disease Cancer Collaboration. Global, Regional, and National Cancer Incidence, Mortality, Years of Life Lost, Years Lived With Disability, and Disability-Adjusted Life-years for 32 Cancer Groups, 1990 to 2015: A Systematic Analysis for the Global Burden of Disease Study. JAMA Oncol. 2017; 3:524–48. https://doi.org/10.1001/jamaoncol.2016.5688 PMID:27918777

2. Saleh K, Eid R, Haddad FG, Khalife-Saleh N, Kourie HR. New developments in the management of head and neck cancer - impact of pembrolizumab. Ther Clin Risk Manag. 2018; 14:295–303. https://doi.org/10.2147/TCRM.S125059 PMID:29497306

3. Zandberg DP, Menk AV, Velez M, Normolle D, DePeaux K, Liu A, Ferris RL, Delgoffe GM. Tumor hypoxia is associated with resistance to PD-1 blockade in squamous cell carcinoma of the head and neck. J Immunother Cancer. 2021; 9:e002088. https://doi.org/10.1136/jitc-2020-002088 PMID:33986123

4. Elmusrati A, Wang J, Wang CY. Tumor microenvironment and immune evasion in head and neck squamous cell carcinoma. Int J Oral Sci. 2021; 13:24. https://doi.org/10.1038/s41368-021-00131-7 PMID:34341329

5. Rugarli EI, Langer T. Mitochondrial quality control: a matter of life and death for neurons. EMBO J. 2012; 31:1336–49. https://doi.org/10.1038/emboj.2012.38 PMID:22354038

6. Okamoto K. Organellophagy: eliminating cellular building blocks via selective autophagy. J Cell Biol. 2014; 205:435–45. https://doi.org/10.1083/jcb.201402054 PMID:24862571

7. Fulda S. Autophagy in Cancer Therapy. Front Oncol. 2017; 7:128. https://doi.org/10.3389/fonc.2017.00128 PMID:28674677

8. Thomas RJ, Oleinik N, Panneer Selvam S, Vaena SG, Dany M, Nganga RN, Depalma R, Baron KD, Kim J, Szulc ZM, Ogretmen B. HPV/E7 induces chemotherapy-mediated tumor suppression by ceramide-dependent mitophagy. EMBO Mol Med. 2017; 9:1030–51. https://doi.org/10.15252/emmm.201607088 PMID:28606997

9. Shen YQ, Guerra-Librero A, Fernandez-Gil BI, Florido J, García-López S, Martinez-Ruiz L, Mendivil-Perez M, Soto-Mercado V, Acuña-Castroviejo D, Ortega-Arellano H, Carriel V, Diaz-Casado ME, Reiter RJ, et al. Combination of melatonin and rapamycin for head and

neck cancer therapy: Suppression of AKT/mTOR pathway activation, and activation of mitophagy and apoptosis via mitochondrial function regulation. J Pineal Res. 2018; 64.
https://doi.org/10.1111/jpi.12461 PMID:29247557

10. Shin YY, Seo Y, Oh SJ, Ahn JS, Song MH, Kang MJ, Oh JM, Lee D, Kim YH, Sung ES, Kim HS. Melatonin and verteporfin synergistically suppress the growth and stemness of head and neck squamous cell carcinoma through the regulation of mitochondrial dynamics. J Pineal Res. 2022; 72:e12779.
https://doi.org/10.1111/jpi.12779 PMID:34826168

11. Onishi M, Yamano K, Sato M, Matsuda N, Okamoto K. Molecular mechanisms and physiological functions of mitophagy. EMBO J. 2021; 40:e104705.
https://doi.org/10.15252/embj.2020104705 PMID:33438778

12. Poole LP, Macleod KF. Mitophagy in tumorigenesis and metastasis. Cell Mol Life Sci. 2021; 78:3817–51.
https://doi.org/10.1007/s00018-021-03774-1 PMID:33580835

13. Scheibye-Knudsen M, Fang EF, Croteau DL, Wilson DM 3rd, Bohr VA. Protecting the mitochondrial powerhouse. Trends Cell Biol. 2015; 25:158–70.
https://doi.org/10.1016/j.tcb.2014.11.002 PMID:25499735

14. Peoples JN, Saraf A, Ghazal N, Pham TT, Kwong JQ. Mitochondrial dysfunction and oxidative stress in heart disease. Exp Mol Med. 2019; 51:1–13.
https://doi.org/10.1038/s12276-019-0355-7 PMID:31857574

15. Bum A. [The patient of the pneumologist in 4 decades. Epidemiologic and socioeconomic viewpoints]. Prax Klin Pneumol. 1988; 42:537–9.
PMID:3186655

16. Vara-Perez M, Felipe-Abrio B, Agostinis P. Mitophagy in Cancer: A Tale of Adaptation. Cells. 2019; 8:493.
https://doi.org/10.3390/cells8050493 PMID:31121959

17. Kulikov AV, Luchkina EA, Gogvadze V, Zhivotovsky B. Mitophagy: Link to cancer development and therapy. Biochem Biophys Res Commun. 2017; 482:432–9.
https://doi.org/10.1016/j.bbrc.2016.10.088 PMID:28212727

18. Gupta A, Anjomani-Virmouni S, Koundouros N, Dimitriadi M, Choo-Wing R, Valle A, Zheng Y, Chiu YH, Agnihotri S, Zadeh G, Asara JM, Anastasiou D, Arends MJ, et al. PARK2 Depletion Connects Energy and Oxidative Stress to PI3K/Akt Activation via PTEN S-Nitrosylation. Mol Cell. 2017; 65:999–1013.e7.
https://doi.org/10.1016/j.molcel.2017.02.019 PMID:28306514

19. Li C, Zhang Y, Cheng X, Yuan H, Zhu S, Liu J, Wen Q, Xie Y, Liu J, Kroemer G, Klionsky DJ, Lotze MT, Zeh HJ, et al. PINK1 and PARK2 Suppress Pancreatic Tumorigenesis through Control of Mitochondrial Iron-Mediated Immunometabolism. Dev Cell. 2018; 46:441–55.e8.
https://doi.org/10.1016/j.devcel.2018.07.012 PMID:30100261

20. Liu K, Li F, Han H, Chen Y, Mao Z, Luo J, Zhao Y, Zheng B, Gu W, Zhao W. Parkin Regulates the Activity of Pyruvate Kinase M2. J Biol Chem. 2016; 291:10307–17.
https://doi.org/10.1074/jbc.M115.703066 PMID:26975375

21. Agnihotri S, Golbourn B, Huang X, Remke M, Younger S, Cairns RA, Chalil A, Smith CA, Krumholtz SL, Mackenzie D, Rakopoulos P, Ramaswamy V, Taccone MS, et al. PINK1 Is a Negative Regulator of Growth and the Warburg Effect in Glioblastoma. Cancer Res. 2016; 76:4708–19.
https://doi.org/10.1158/0008-5472.CAN-15-3079 PMID:27325644

22. Chourasia AH, Boland ML, Macleod KF. Mitophagy and cancer. Cancer Metab. 2015; 3:4.
https://doi.org/10.1186/s40170-015-0130-8 PMID:25810907

23. Naik PP, Birbrair A, Bhutia SK. Mitophagy-driven metabolic switch reprograms stem cell fate. Cell Mol Life Sci. 2019; 76:27–43.
https://doi.org/10.1007/s00018-018-2922-9 PMID:30267101

24. Adams WC, Chen YH, Kratchmarov R, Yen B, Nish SA, Lin WW, Rothman NJ, Luchsinger LL, Klein U, Busslinger M, Rathmell JC, Snoeck HW, Reiner SL. Anabolism-Associated Mitochondrial Stasis Driving Lymphocyte Differentiation over Self-Renewal. Cell Rep. 2016; 17:3142–52.
https://doi.org/10.1016/j.celrep.2016.11.065 PMID:28009285

25. Ito K, Turcotte R, Cui J, Zimmerman SE, Pinho S, Mizoguchi T, Arai F, Runnels JM, Alt C, Teruya-Feldstein J, Mar JC, Singh R, Suda T, et al. Self-renewal of a purified Tie2+ hematopoietic stem cell population relies on mitochondrial clearance. Science. 2016; 354:1156–60.
https://doi.org/10.1126/science.aaf5530 PMID:27738012

26. Liu K, Lee J, Kim JY, Wang L, Tian Y, Chan ST, Cho C, Machida K, Chen D, Ou JJ. Mitophagy Controls the Activities of Tumor Suppressor p53 to Regulate Hepatic Cancer Stem Cells. Mol Cell. 2017; 68:281–92.e5.
https://doi.org/10.1016/j.molcel.2017.09.022 PMID:29033320

27. Snyder V, Reed-Newman TC, Arnold L, Thomas SM, Anant S. Cancer Stem Cell Metabolism and Potential Therapeutic Targets. Front Oncol. 2018; 8:203. https://doi.org/10.3389/fonc.2018.00203 PMID:29922594

28. Shen YA, Wang CY, Hsieh YT, Chen YJ, Wei YH. Metabolic reprogramming orchestrates cancer stem cell properties in nasopharyngeal carcinoma. Cell Cycle. 2015; 14:86–98. https://doi.org/10.4161/15384101.2014.974419 PMID:25483072

29. Naik PP, Mukhopadhyay S, Panda PK, Sinha N, Das CK, Mishra R, Patil S, Bhutia SK. Autophagy regulates cisplatin-induced stemness and chemoresistance via the upregulation of CD44, ABCB1 and ADAM17 in oral squamous cell carcinoma. Cell Prolif. 2018; 51:e12411. https://doi.org/10.1111/cpr.12411 PMID:29171106

30. Tomczak K, Czerwińska P, Wiznerowicz M. The Cancer Genome Atlas (TCGA): an immeasurable source of knowledge. Contemp Oncol (Pozn). 2015; 19:A68–77. https://doi.org/10.5114/wo.2014.47136 PMID:25691825

31. Liberzon A, Subramanian A, Pinchback R, Thorvaldsdóttir H, Tamayo P, Mesirov JP. Molecular signatures database (MSigDB) 3.0. Bioinformatics. 2011; 27:1739–40. https://doi.org/10.1093/bioinformatics/btr260 PMID:21546393

32. Jassal B, Matthews L, Viteri G, Gong C, Lorente P, Fabregat A, Sidiropoulos K, Cook J, Gillespie M, Haw R, Loney F, May B, Milacic M, et al. The reactome pathway knowledgebase. Nucleic Acids Res. 2020; 48:D498–503. https://doi.org/10.1093/nar/gkz1031 PMID:31691815

33. Kamburov A, Wierling C, Lehrach H, Herwig R. ConsensusPathDB--a database for integrating human functional interaction networks. Nucleic Acids Res. 2009; 37:D623–8. https://doi.org/10.1093/nar/gkn698 PMID:18940869

34. Kanehisa M, Goto S. KEGG: kyoto encyclopedia of genes and genomes. Nucleic Acids Res. 2000; 28:27–30. https://doi.org/10.1093/nar/28.1.27 PMID:10592173

35. Wilkerson MD, Hayes DN. ConsensusClusterPlus: a class discovery tool with confidence assessments and item tracking. Bioinformatics. 2010; 26:1572–3. https://doi.org/10.1093/bioinformatics/btq170 PMID:20427518

36. Li T, Fan J, Wang B, Traugh N, Chen Q, Liu JS, Li B, Liu XS. TIMER: A Web Server for Comprehensive Analysis of Tumor-Infiltrating Immune Cells. Cancer Res. 2017; 77:e108–10. https://doi.org/10.1158/0008-5472.CAN-17-0307 PMID:29092952

37. Chen B, Khodadoust MS, Liu CL, Newman AM, Alizadeh AA. Profiling Tumor Infiltrating Immune Cells with CIBERSORT. Methods Mol Biol. 2018; 1711:243–59. https://doi.org/10.1007/978-1-4939-7493-1_12 PMID:29344893

38. Aran D, Hu Z, Butte AJ. xCell: digitally portraying the tissue cellular heterogeneity landscape. Genome Biol. 2017; 18:220. https://doi.org/10.1186/s13059-017-1349-1 PMID:29141660

39. Racle J, Gfeller D. EPIC: A Tool to Estimate the Proportions of Different Cell Types from Bulk Gene Expression Data. Methods Mol Biol. 2020; 2120:233–48. https://doi.org/10.1007/978-1-0716-0327-7_17 PMID:32124324

40. Mayakonda A, Lin DC, Assenov Y, Plass C, Koeffler HP. Maftools: efficient and comprehensive analysis of somatic variants in cancer. Genome Res. 2018; 28:1747–56. https://doi.org/10.1101/gr.239244.118 PMID:30341162

41. Jiang A, Meng J, Bao Y, Wang A, Gong W, Gan X, Wang J, Bao Y, Wu Z, Lu J, Liu B, Wang L. Establishment of a prognosis Prediction Model Based on Pyroptosis-Related Signatures Associated With the Immune Microenvironment and Molecular Heterogeneity in Clear Cell Renal Cell Carcinoma. Front Oncol. 2021; 11:755212. https://doi.org/10.3389/fonc.2021.755212 PMID:34804944

42. Mermel CH, Schumacher SE, Hill B, Meyerson ML, Beroukhim R, Getz G. GISTIC2.0 facilitates sensitive and confident localization of the targets of focal somatic copy-number alteration in human cancers. Genome Biol. 2011; 12:R41. https://doi.org/10.1186/gb-2011-12-4-r41 PMID:21527027

43. Yang W, Soares J, Greninger P, Edelman EJ, Lightfoot H, Forbes S, Bindal N, Beare D, Smith JA, Thompson IR, Ramaswamy S, Futreal PA, Haber DA, et al. Genomics of Drug Sensitivity in Cancer (GDSC): a resource for therapeutic biomarker discovery in cancer cells. Nucleic Acids Res. 2013; 41:D955–61. https://doi.org/10.1093/nar/gks1111 PMID:23180760

44. Maeser D, Gruener RF, Huang RS. oncoPredict: an R package for predicting *in vivo* or cancer patient drug response and biomarkers from cell line screening data. Brief Bioinform. 2021; 22:bbab260. https://doi.org/10.1093/bib/bbab260 PMID:34260682

45. Reinhold WC, Sunshine M, Liu H, Varma S, Kohn KW, Morris J, Doroshow J, Pommier Y. CellMiner: a web-based suite of genomic and pharmacologic tools to explore transcript and drug patterns in the NCI-60 cell line set. Cancer Res. 2012; 72:3499–511. https://doi.org/10.1158/0008-5472.CAN-12-1370 PMID:22802077

46. Barretina J, Caponigro G, Stransky N, Venkatesan K, Margolin AA, Kim S, Wilson CJ, Lehár J, Kryukov GV, Sonkin D, Reddy A, Liu M, Murray L, et al. The Cancer Cell Line Encyclopedia enables predictive modelling of anticancer drug sensitivity. Nature. 2012; 483:603–7. https://doi.org/10.1038/nature11003 PMID:22460905

47. Efremova M, Vento-Tormo M, Teichmann SA, Vento-Tormo R. CellPhoneDB: inferring cell-cell communication from combined expression of multi-subunit ligand-receptor complexes. Nat Protoc. 2020; 15:1484–506. https://doi.org/10.1038/s41596-020-0292-x PMID:32103204

48. Fu J, Li K, Zhang W, Wan C, Zhang J, Jiang P, Liu XS. Large-scale public data reuse to model immunotherapy response and resistance. Genome Med. 2020; 12:21. https://doi.org/10.1186/s13073-020-0721-z PMID:32102694

49. Jiang P, Gu S, Pan D, Fu J, Sahu A, Hu X, Li Z, Traugh N, Bu X, Li B, Liu J, Freeman GJ, Brown MA, et al. Signatures of T cell dysfunction and exclusion predict cancer immunotherapy response. Nat Med. 2018; 24:1550–8. https://doi.org/10.1038/s41591-018-0136-1 PMID:30127393

50. Chen Z, Luo Z, Zhang D, Li H, Liu X, Zhu K, Zhang H, Wang Z, Zhou P, Ren J, Zhao A, Zuo Z. TIGER: A Web Portal of Tumor Immunotherapy Gene Expression Resource. Genomics Proteomics Bioinformatics. 2023; 21:337–48. https://doi.org/10.1016/j.gpb.2022.08.004 PMID:36049666

51. Hatfield SM, Kjaergaard J, Lukashev D, Schreiber TH, Belikoff B, Abbott R, Sethumadhavan S, Philbrook P, Ko K, Cannici R, Thayer M, Rodig S, Kutok JL, et al. Immunological mechanisms of the antitumor effects of supplemental oxygenation. Sci Transl Med. 2015; 7:277ra30. https://doi.org/10.1126/scitranslmed.aaa1260 PMID:25739764

52. Scharping NE, Menk AV, Whetstone RD, Zeng X, Delgoffe GM. Efficacy of PD-1 Blockade Is Potentiated by Metformin-Induced Reduction of Tumor Hypoxia. Cancer Immunol Res. 2017; 5:9–16. https://doi.org/10.1158/2326-6066.CIR-16-0103 PMID:27941003

53. Abou Khouzam R, Goutham HV, Zaarour RF, Chamseddine AN, Francis A, Buart S, Terry S, Chouaib S. Integrating tumor hypoxic stress in novel and more adaptable strategies for cancer immunotherapy. Semin Cancer Biol. 2020; 65:140–54. https://doi.org/10.1016/j.semcancer.2020.01.003 PMID:31927131

54. Chagas VS, Groeneveld CS, Oliveira KG, Trefflich S, de Almeida RC, Ponder BAJ, Meyer KB, Jones SJM, Robertson AG, Castro MA. RTNduals: an R/Bioconductor package for analysis of co-regulation and inference of dual regulons. Bioinformatics. 2019; 35:5357–8. https://doi.org/10.1093/bioinformatics/btz534 PMID:31250887

55. Makita S, Takatori H, Nakajima H. Post-Transcriptional Regulation of Immune Responses and Inflammatory Diseases by RNA-Binding ZFP36 Family Proteins. Front Immunol. 2021; 12:711633. https://doi.org/10.3389/fimmu.2021.711633 PMID:34276705

56. Liu L, Zuo Z, Lu S, Wang L, Liu A, Liu X. Silencing of PINK1 represses cell growth, migration and induces apoptosis of lung cancer cells. Biomed Pharmacother. 2018; 106:333–41. https://doi.org/10.1016/j.biopha.2018.06.128 PMID:29966978

57. Tay SP, Yeo CW, Chai C, Chua PJ, Tan HM, Ang AX, Yip DL, Sung JX, Tan PH, Bay BH, Wong SH, Tang C, Tan JM, Lim KL. Parkin enhances the expression of cyclin-dependent kinase 6 and negatively regulates the proliferation of breast cancer cells. J Biol Chem. 2010; 285:29231–8. https://doi.org/10.1074/jbc.M110.108241 PMID:20630868

58. Tan EY, Campo L, Han C, Turley H, Pezzella F, Gatter KC, Harris AL, Fox SB. BNIP3 as a progression marker in primary human breast cancer; opposing functions in *in situ* versus invasive cancer. Clin Cancer Res. 2007; 13:467–74. https://doi.org/10.1158/1078-0432.CCR-06-1466 PMID:17255267

59. Hui L, Wu H, Wang TW, Yang N, Guo X, Jang XJ. Hydrogen peroxide-induced mitophagy contributes to laryngeal cancer cells survival via the upregulation of FUNDC1. Clin Transl Oncol. 2019; 21:596–606. https://doi.org/10.1007/s12094-018-1958-5 PMID:30284230

60. Yan C, Li TS. Dual Role of Mitophagy in Cancer Drug Resistance. Anticancer Res. 2018; 38:617–21. https://doi.org/10.21873/anticanres.12266 PMID:29374684

61. Yamashita K, Miyata H, Makino T, Masuike Y, Furukawa H, Tanaka K, Miyazaki Y, Takahashi T, Kurokawa Y, Yamasaki M, Nakajima K, Takiguchi S, Morii E, et al. High Expression of the Mitophagy-Related Protein Pink1 is Associated with a Poor Response to Chemotherapy and a Poor Prognosis for Patients Treated with Neoadjuvant Chemotherapy for Esophageal Squamous Cell Carcinoma. Ann Surg Oncol. 2017; 24:4025–32. https://doi.org/10.1245/s10434-017-6096-8 PMID:29022200

62. Zhou J, Li G, Zheng Y, Shen HM, Hu X, Ming QL, Huang C, Li P, Gao N. A novel autophagy/mitophagy inhibitor liensinine sensitizes breast cancer cells to chemotherapy through DNM1L-mediated mitochondrial fission. Autophagy. 2015; 11:1259–79. https://doi.org/10.1080/15548627.2015.1056970 PMID:26114658

63. Liu J, Zhang C, Zhao Y, Yue X, Wu H, Huang S, Chen J, Tomsky K, Xie H, Khella CA, Gatza ML, Xia D, Gao J, et al. Parkin targets HIF-1α for ubiquitination and degradation to inhibit breast tumor progression. Nat Commun. 2017; 8:1823. https://doi.org/10.1038/s41467-017-01947-w PMID:29180628

64. Sena LA, Chandel NS. Physiological roles of mitochondrial reactive oxygen species. Mol Cell. 2012; 48:158–67. https://doi.org/10.1016/j.molcel.2012.09.025 PMID:23102266

65. Zhong Z, Umemura A, Sanchez-Lopez E, Liang S, Shalapour S, Wong J, He F, Boassa D, Perkins G, Ali SR, McGeough MD, Ellisman MH, Seki E, et al. NF-κB Restricts Inflammasome Activation via Elimination of Damaged Mitochondria. Cell. 2016; 164:896–910. https://doi.org/10.1016/j.cell.2015.12.057 PMID:26919428

66. Naik PP, Das DN, Panda PK, Mukhopadhyay S, Sinha N, Praharaj PP, Agarwal R, Bhutia SK. Implications of cancer stem cells in developing therapeutic resistance in oral cancer. Oral Oncol. 2016; 62:122–35. https://doi.org/10.1016/j.oraloncology.2016.10.008 PMID:27865365

67. Tang YC, Hsiao JR, Jiang SS, Chang JY, Chu PY, Liu KJ, Fang HL, Lin LM, Chen HH, Huang YW, Chen YT, Tsai FY, Lin SF, et al. c-MYC-directed NRF2 drives malignant progression of head and neck cancer via glucose-6-phosphate dehydrogenase and transketolase activation. Theranostics. 2021; 11:5232–47. https://doi.org/10.7150/thno.53417 PMID:33859744

68. Pak K, Cheon GJ, Nam HY, Kim SJ, Kang KW, Chung JK, Kim EE, Lee DS. Prognostic value of metabolic tumor volume and total lesion glycolysis in head and neck cancer: a systematic review and meta-analysis. J Nucl Med. 2014; 55:884–90. https://doi.org/10.2967/jnumed.113.133801 PMID:24752671

69. Qiu Z, Guo W, Dong B, Wang Y, Deng P, Wang C, Liu J, Zhang Q, Grosschedl R, Yu Z, Deng J, Wu Y. EBF1 promotes triple-negative breast cancer progression by surveillance of the HIF1α pathway. Proc Natl Acad Sci USA. 2022; 119:e2119518119. https://doi.org/10.1073/pnas.2119518119 PMID:35867755

70. Pan XC, Xiong YL, Hong JH, Liu Y, Cen YY, Liu T, Yang QF, Tao H, Li YN, Zhang HG. Cardiomyocytic FoxP3 is involved in Parkin-mediated mitophagy during cardiac remodeling and the regulatory role of triptolide. Theranostics. 2022; 12:2483–501. https://doi.org/10.7150/thno.71102 PMID:35265221

71. Mandal R, Şenbabaoğlu Y, Desrichard A, Havel JJ, Dalin MG, Riaz N, Lee KW, Ganly I, Hakimi AA, Chan TA, Morris LG. The head and neck cancer immune landscape and its immunotherapeutic implications. JCI Insight. 2016; 1:e89829. https://doi.org/10.1172/jci.insight.89829 PMID:27777979

72. Whiteside TL. Immunobiology of head and neck cancer. Cancer Metastasis Rev. 2005; 24:95–105. https://doi.org/10.1007/s10555-005-5050-6 PMID:15785875

73. Wagner S, Wittekindt C, Reuschenbach M, Hennig B, Thevarajah M, Würdemann N, Prigge ES, von Knebel Doeberitz M, Dreyer T, Gattenlöhner S, Klussmann JP. CD56-positive lymphocyte infiltration in relation to human papillomavirus association and prognostic significance in oropharyngeal squamous cell carcinoma. Int J Cancer. 2016; 138:2263–73. https://doi.org/10.1002/ijc.29962 PMID:26662627

74. Agarwal R, Chaudhary M, Bohra S, Bajaj S. Evaluation of natural killer cell (CD57) as a prognostic marker in oral squamous cell carcinoma: An immunohistochemistry study. J Oral Maxillofac Pathol. 2016; 20:173–7. https://doi.org/10.4103/0973-029X.185933 PMID:27601804

75. Vasquez-Dunddel D, Pan F, Zeng Q, Gorbounov M, Albesiano E, Fu J, Blosser RL, Tam AJ, Bruno T, Zhang H, Pardoll D, Kim Y. STAT3 regulates arginase-I in myeloid-derived suppressor cells from cancer patients. J Clin Invest. 2013; 123:1580–9. https://doi.org/10.1172/JCI60083 PMID:23454751

76. Trellakis S, Bruderek K, Dumitru CA, Gholaman H, Gu X, Bankfalvi A, Scherag A, Hütte J, Dominas N, Lehnerdt GF, Hoffmann TK, Lang S, Brandau S. Polymorphonuclear granulocytes in human head

and neck cancer: enhanced inflammatory activity, modulation by cancer cells and expansion in advanced disease. Int J Cancer. 2011; 129:2183–93. https://doi.org/10.1002/ijc.25892 PMID:21190185

77. Costa NL, Valadares MC, Souza PP, Mendonça EF, Oliveira JC, Silva TA, Batista AC. Tumor-associated macrophages and the profile of inflammatory cytokines in oral squamous cell carcinoma. Oral Oncol. 2013; 49:216–23. https://doi.org/10.1016/j.oraloncology.2012.09.012 PMID:23089461

78. Dinarello CA. Immunological and inflammatory functions of the interleukin-1 family. Annu Rev Immunol. 2009; 27:519–50. https://doi.org/10.1146/annurev.immunol.021908.132612 PMID:19302047

79. Sims JE, Smith DE. The IL-1 family: regulators of immunity. Nat Rev Immunol. 2010; 10:89–102. https://doi.org/10.1038/nri2691 PMID:20081871

80. Garlanda C, Dinarello CA, Mantovani A. The interleukin-1 family: back to the future. Immunity. 2013; 39:1003–18. https://doi.org/10.1016/j.immuni.2013.11.010 PMID:24332029

81. Saitoh T, Fujita N, Jang MH, Uematsu S, Yang BG, Satoh T, Omori H, Noda T, Yamamoto N, Komatsu M, Tanaka K, Kawai T, Tsujimura T, et al. Loss of the autophagy protein Atg16L1 enhances endotoxin-induced IL-1beta production. Nature. 2008; 456:264–8. https://doi.org/10.1038/nature07383 PMID:18849965

82. Zhou R, Yazdi AS, Menu P, Tschopp J. A role for mitochondria in NLRP3 inflammasome activation. Nature. 2011; 469:221–5. https://doi.org/10.1038/nature09663 PMID:21124315

83. Nakahira K, Haspel JA, Rathinam VA, Lee SJ, Dolinay T, Lam HC, Englert JA, Rabinovitch M, Cernadas M, Kim HP, Fitzgerald KA, Ryter SW, Choi AM. Autophagy proteins regulate innate immune responses by inhibiting the release of mitochondrial DNA mediated by the NALP3 inflammasome. Nat Immunol. 2011; 12:222–30. https://doi.org/10.1038/ni.1980 PMID:21151103

84. Harris J, Hartman M, Roche C, Zeng SG, O'Shea A, Sharp FA, Lambe EM, Creagh EM, Golenbock DT, Tschopp J, Kornfeld H, Fitzgerald KA, Lavelle EC. Autophagy controls IL-1beta secretion by targeting pro-IL-1beta for degradation. J Biol Chem. 2011; 286:9587–97. https://doi.org/10.1074/jbc.M110.202911 PMID:21228274

85. Ivashkiv LB, Donlin LT. Regulation of type I interferon responses. Nat Rev Immunol. 2014; 14:36–49. https://doi.org/10.1038/nri3581 PMID:24362405

86. Tal MC, Sasai M, Lee HK, Yordy B, Shadel GS, Iwasaki A. Absence of autophagy results in reactive oxygen species-dependent amplification of RLR signaling. Proc Natl Acad Sci USA. 2009; 106:2770–5. https://doi.org/10.1073/pnas.0807694106 PMID:19196953

87. Jia W, Pua HH, Li QJ, He YW. Autophagy regulates endoplasmic reticulum homeostasis and calcium mobilization in T lymphocytes. J Immunol. 2011; 186:1564–74. https://doi.org/10.4049/jimmunol.1001822 PMID:21191072

88. Salio M, Puleston DJ, Mathan TS, Shepherd D, Stranks AJ, Adamopoulou E, Veerapen N, Besra GS, Hollander GA, Simon AK, Cerundolo V. Essential role for autophagy during invariant NKT cell development. Proc Natl Acad Sci USA. 2014; 111:E5678–87. https://doi.org/10.1073/pnas.1413935112 PMID:25512546

89. O'Sullivan TE, Johnson LR, Kang HH, Sun JC. BNIP3- and BNIP3L-Mediated Mitophagy Promotes the Generation of Natural Killer Cell Memory. Immunity. 2015; 43:331–42. https://doi.org/10.1016/j.immuni.2015.07.012 PMID:26253785

90. Ip WKE, Hoshi N, Shouval DS, Snapper S, Medzhitov R. Anti-inflammatory effect of IL-10 mediated by metabolic reprogramming of macrophages. Science. 2017; 356:513–9. https://doi.org/10.1126/science.aal3535 PMID:28473584

91. Patel J. IL-10 reprogramming of metabolism in macrophages through mitophagy. Cardiovasc Res. 2017; 113:e40–1. https://doi.org/10.1093/cvr/cvx144 PMID:28859306

92. Zhao Y, Guo Y, Jiang Y, Zhu X, Liu Y, Zhang X. Mitophagy regulates macrophage phenotype in diabetic nephropathy rats. Biochem Biophys Res Commun. 2017; 494:42–50. https://doi.org/10.1016/j.bbrc.2017.10.088 PMID:29061302

93. Kim JM, Chen DS. Immune escape to PD-L1/PD-1 blockade: seven steps to success (or failure). Ann Oncol. 2016; 27:1492–504. https://doi.org/10.1093/annonc/mdw217 PMID:27207108

94. Dhodapkar KM, Dhodapkar MV. Recruiting dendritic cells to improve antibody therapy of cancer. Proc Natl Acad Sci USA. 2005; 102:6243–4. https://doi.org/10.1073/pnas.0502547102 PMID:15851655

95. Chen Y, Chen C. DNA copy number variation and loss of heterozygosity in relation to recurrence of and survival from head and neck squamous cell carcinoma: a review. Head Neck. 2008; 30:1361–83. https://doi.org/10.1002/hed.20861 PMID:18642290

96. Yao N, Wang C, Hu N, Li Y, Liu M, Lei Y, Chen M, Chen L, Chen C, Lan P, Chen W, Chen Z, Fu D, et al. Inhibition of PINK1/Parkin-dependent mitophagy sensitizes multidrug-resistant cancer cells to B5G1, a new betulinic acid analog. Cell Death Dis. 2019; 10:232. https://doi.org/10.1038/s41419-019-1470-z PMID:30850585

SUPPLEMENTARY MATERIALS

Supplementary Figures

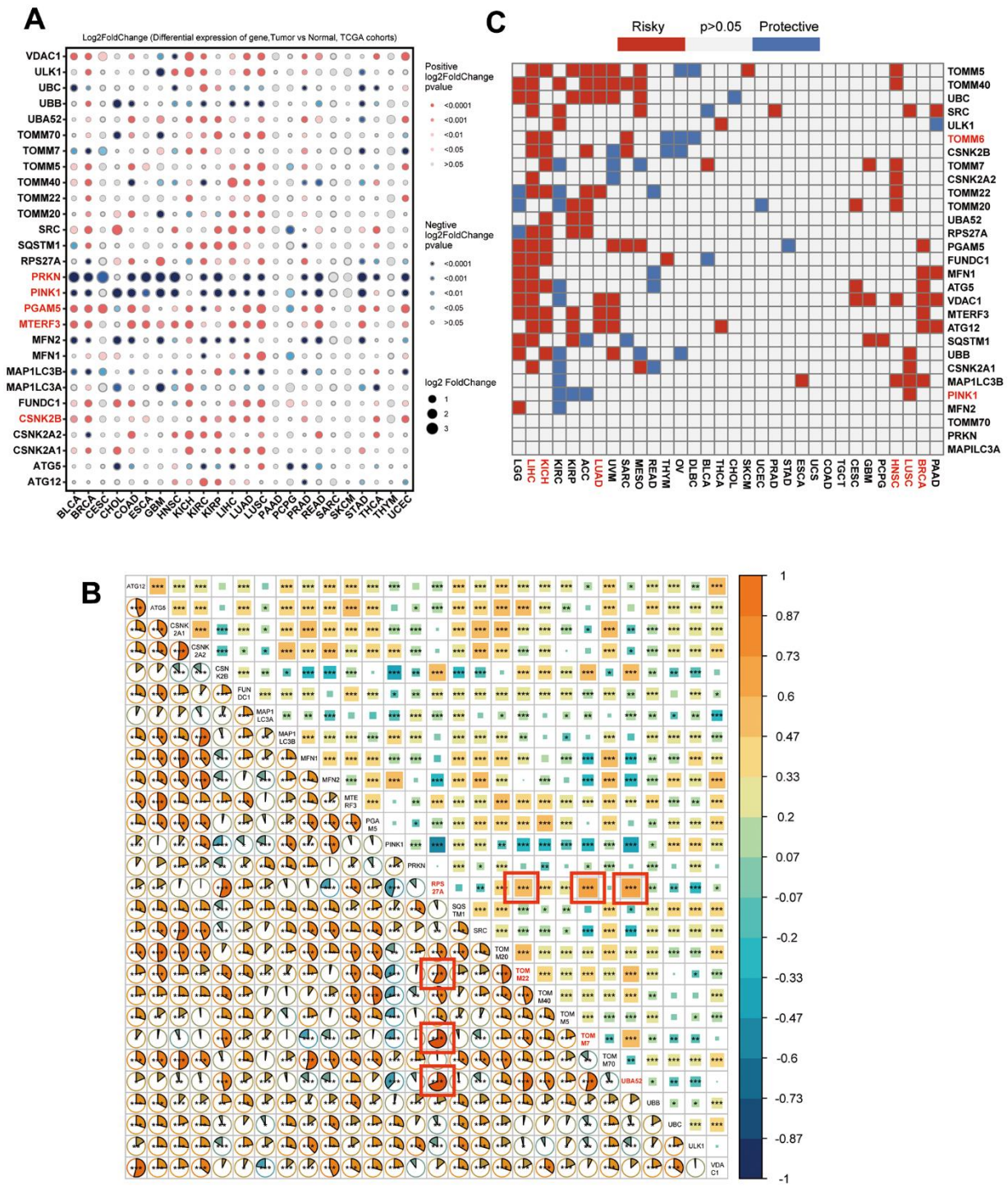

Supplementary Figure 1. Disrupted mitophagy regulators in cancers and correlations with patient outcomes: (**A**) mRNA expression related to mitophagy in multiple cancers. (**B**) The correlation of mitophagy-related genes in the expression matrix TCGA-HNSC using two methods, Spearman (upper right) and Pearson (lower left) correlation tests. (**C**) The association between transcript levels and patient outcomes.

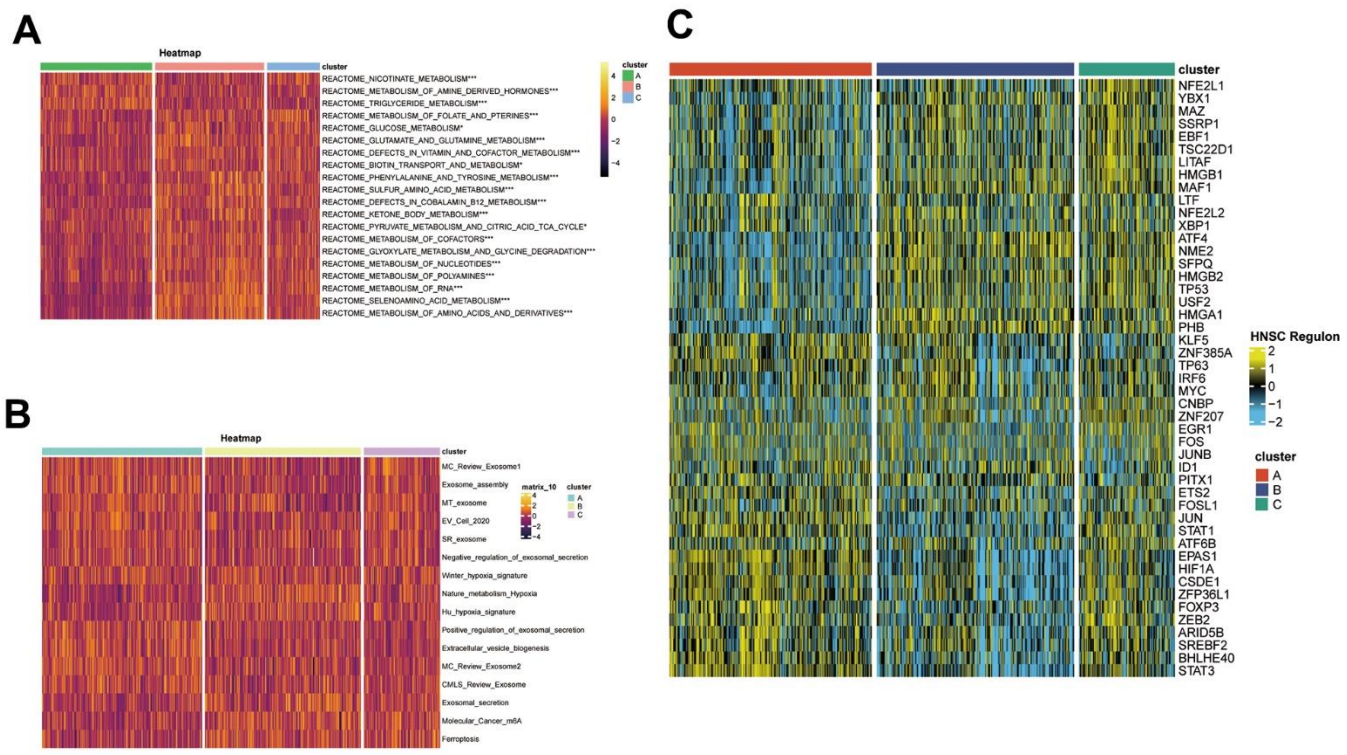

Supplementary Figure 2. Functional Enrichment Analysis in Distinct Mitophagy Modification Patterns: (**A**, **B**) Heatmap of metabolism-related and cancer-related pathway enrichment scores among the subtypes by GSVA analysis. (**C**) Heatmap of transcription factor regulon activation in three mitophagy modification subtypes. ****P < 0.0001, ***P < 0.001, **P < 0.01, *P < 0.05

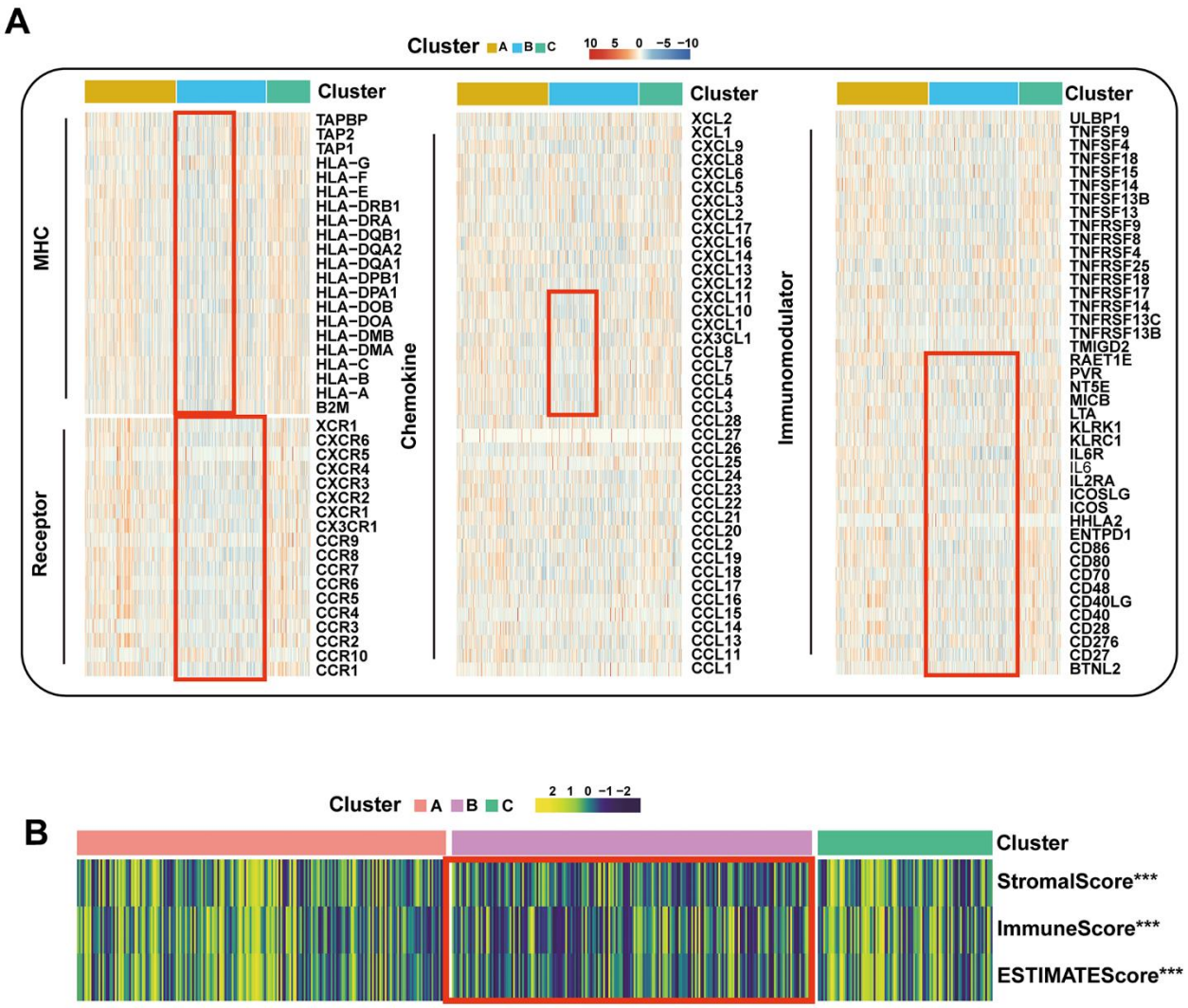

Supplementary Figure 3. Comparison of the Specific Immune Infiltration Landscape among Three Subgroups: (**A**) Heatmap of chemokines, chemokine receptors, immunoinhibitors, and immunostimulators among the subtypes by expression analysis. (**B**) Heatmap of estimate score in three mitophagy modification subtypes. ****P < 0.0001, ***P < 0.001, **P < 0.01, *P < 0.05.

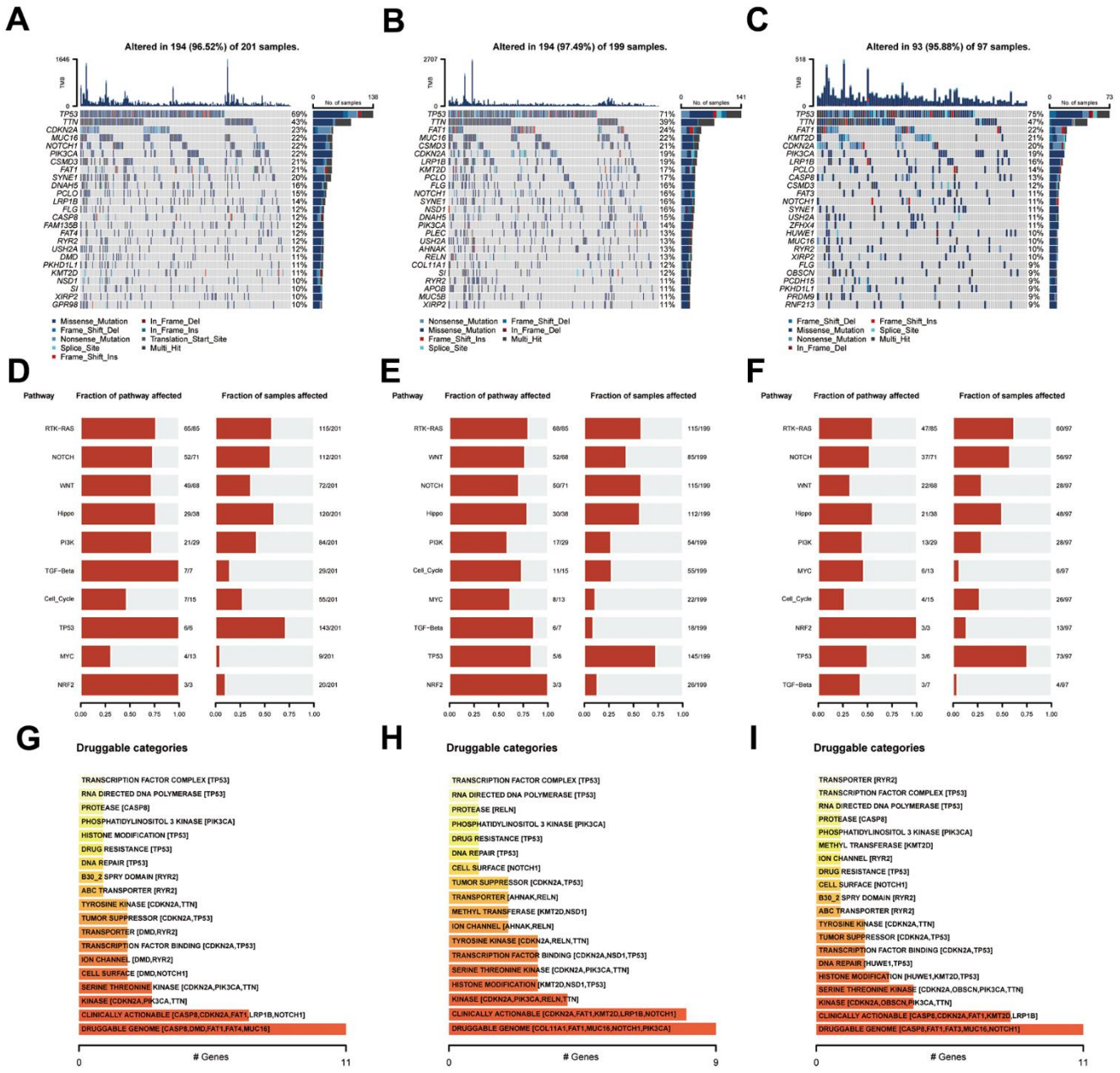

Supplementary Figure 4. Landscapes of somatic mutation among subgroups: (**A**–**C**) Waterfall plot showing the mutation patterns of the top 20 most frequently mutated genes. Each column represented patients. The upper barplot showed tumor mutational burden. The mutation frequency of each gene was indicated on the right. (**D**–**F**) Potentially druggable gene categories from mutation datasets in Cluster A, B, and C. (**G**–**I**) Onco-pathway alteration frequency and the fraction of sample affected for each pathway in Cluster A, B, and C.

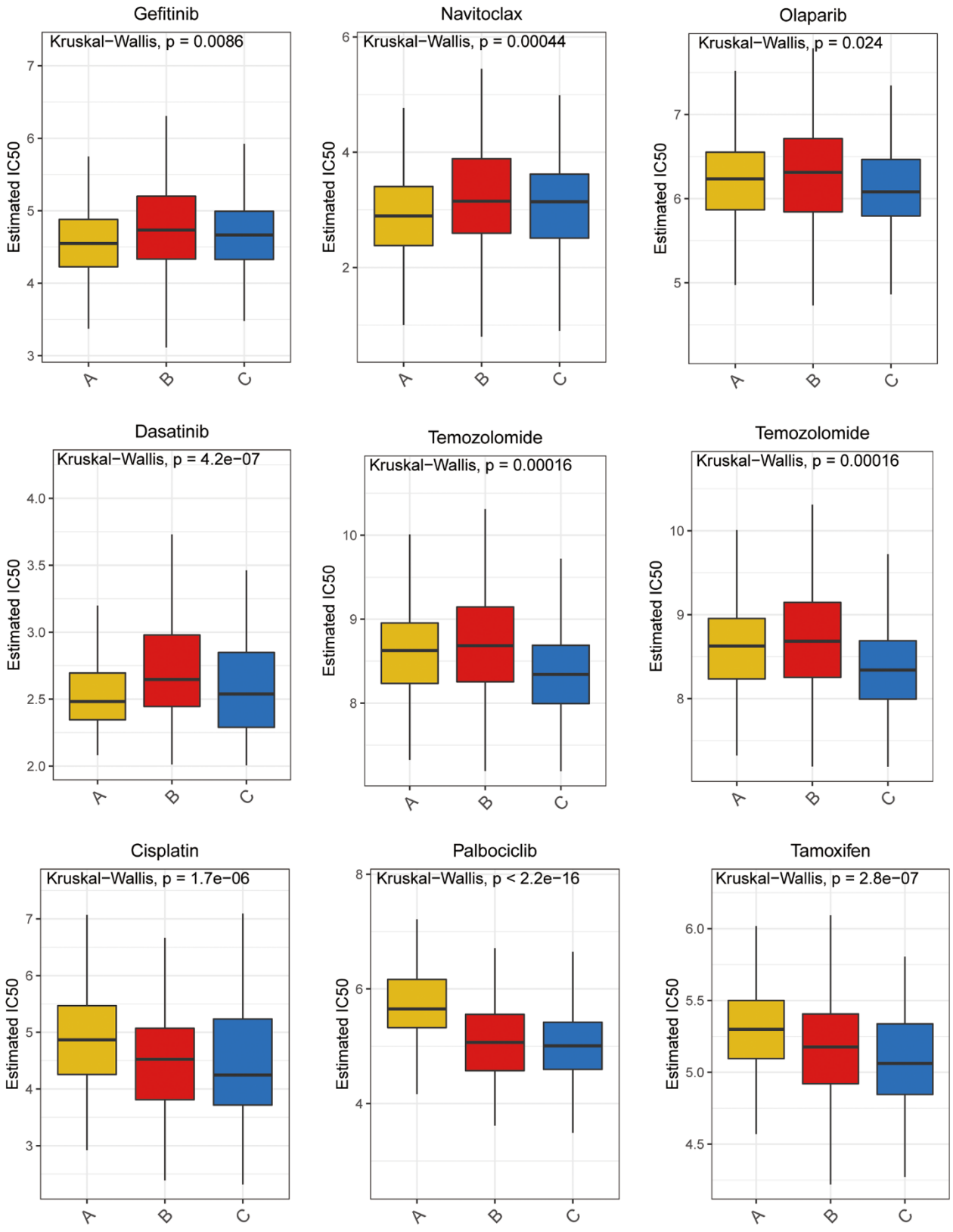

Supplementary Figure 5. Comparison of drug sensitivity. Estimated IC50 of the indicated molecular targeted drugs in Cluster A, B, and C.

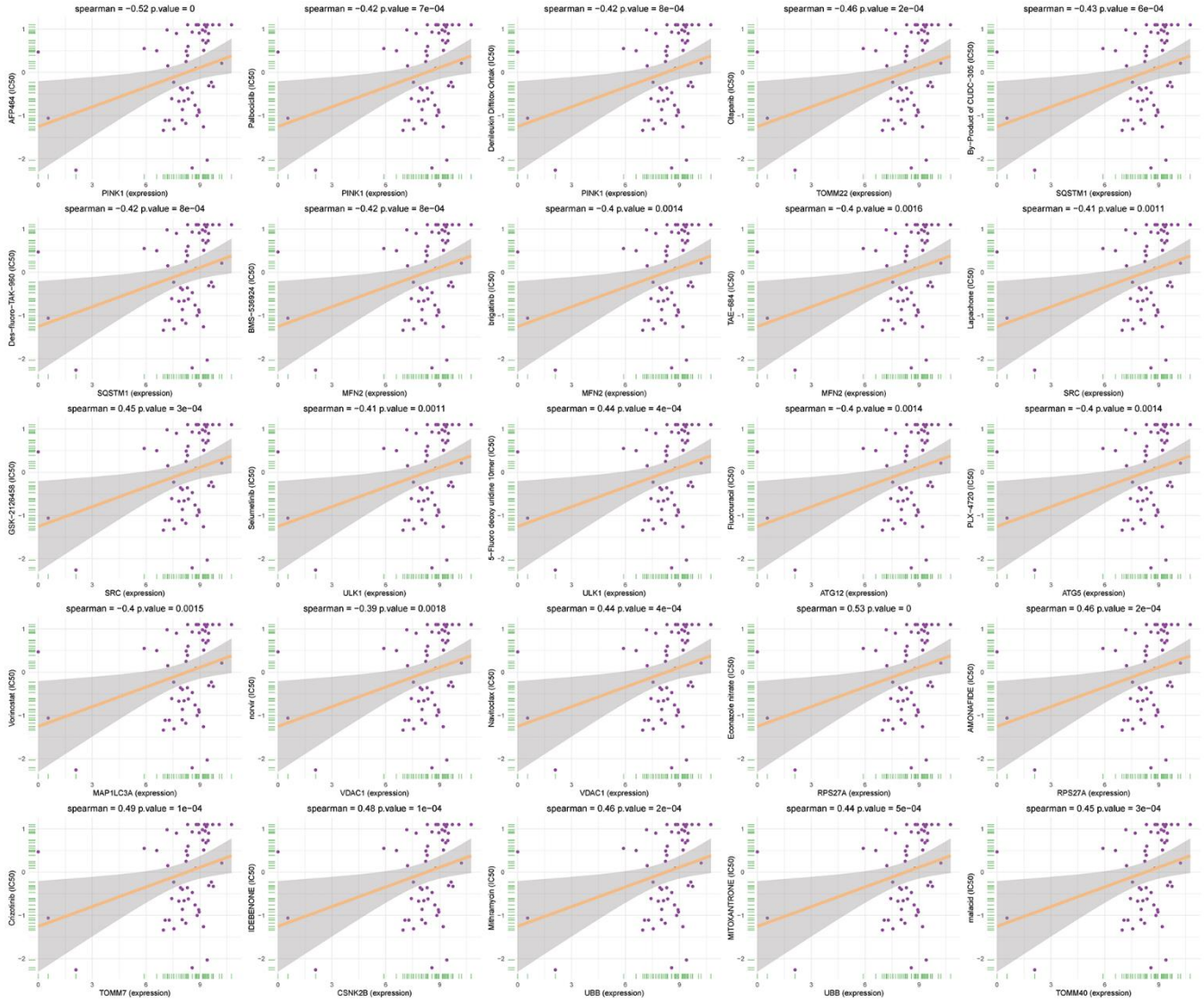

Supplementary Figure 6. The association between mitophagy gene expression and drug sensitivity based on the CellMiner database.

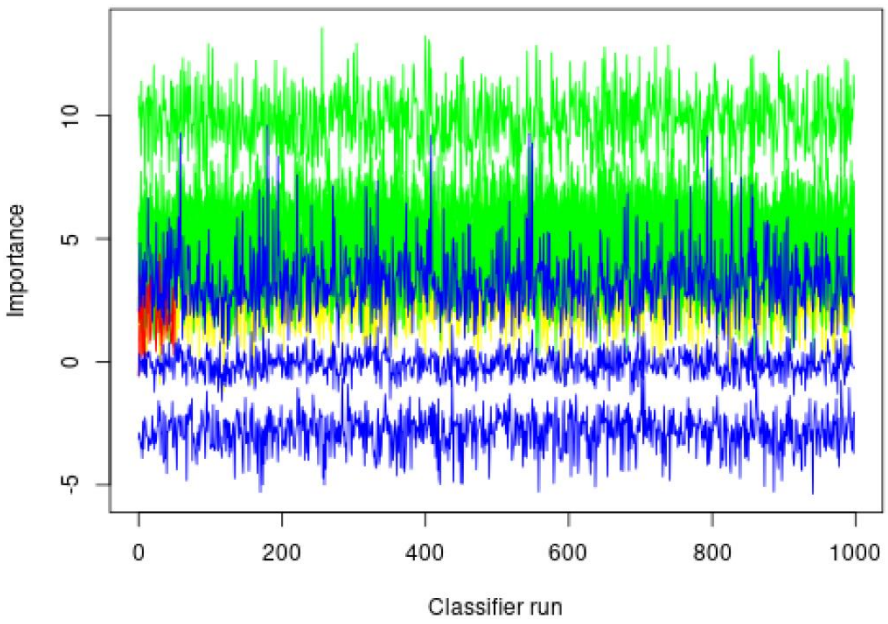

Supplementary Figure 7. Results of the Boruta algorithm iterations. Green indicates features considered important by the Boruta algorithm while blue represents shadow attributes.

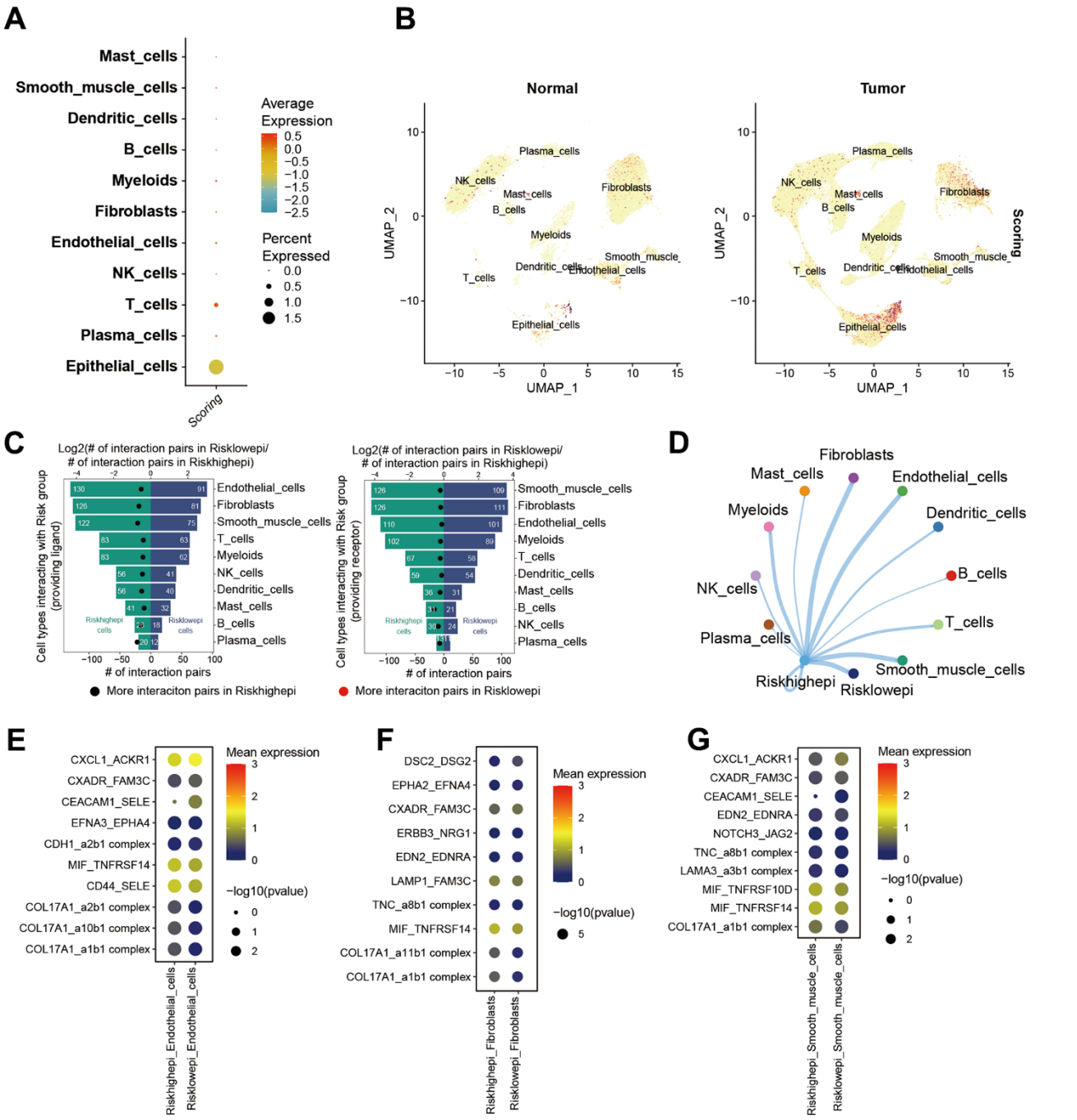

Supplementary Figure 8. Observations on cell-to- cell communication. (**A**) Scores for each cell type shown in a dotplot. (**B**) Dimensionality reduction charts show the risk scores of different cell types, grouped by normal and tumor. (**C**) Overview of cellular communication. (**D**) Network visualization of high-risk epigenetic profiles' communication patterns. (**E**–**G**) Bubble plots depicting communication intensity between various cell types and the Risk group. This includes interactions from the Risk group to Endothelial cells (**E**), Fibroblasts (**F**), and Smooth muscle cells (**G**) to the Risk group.

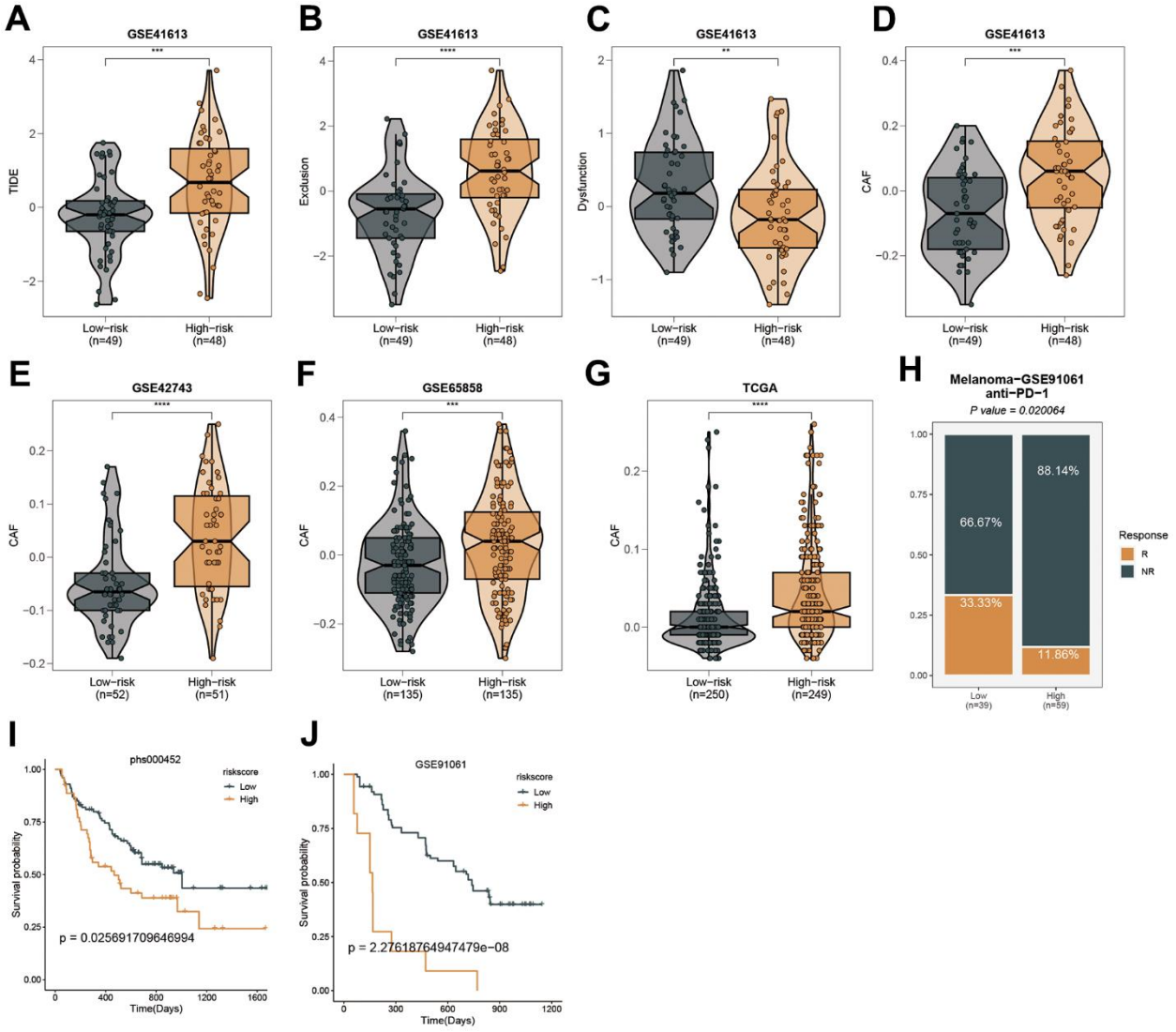

Supplementary Figure 9. Predicting immune therapy response with MSRS. (**A**–**C**) Comparison of the TIDE (**A**), dysfunction (**B**), and exclusion (**C**) between groups with high and low MSRS. (**D**–**G**) Comparison of CAF in high and low MSRS groups in GSE41613 (**D**), GSE42743 (**E**), GSE65858 (**F**), and TCGA (**G**). (**H**) A comparison of the MSRS between immune therapy responders and nonresponders in the GSE91061 immunotherapy cohort. (**I**, **J**) Based on the phs000452 (**I**), and GSE91061 (**J**) immunotherapy cohorts, the effect of MSRS on prognosis in these patients.

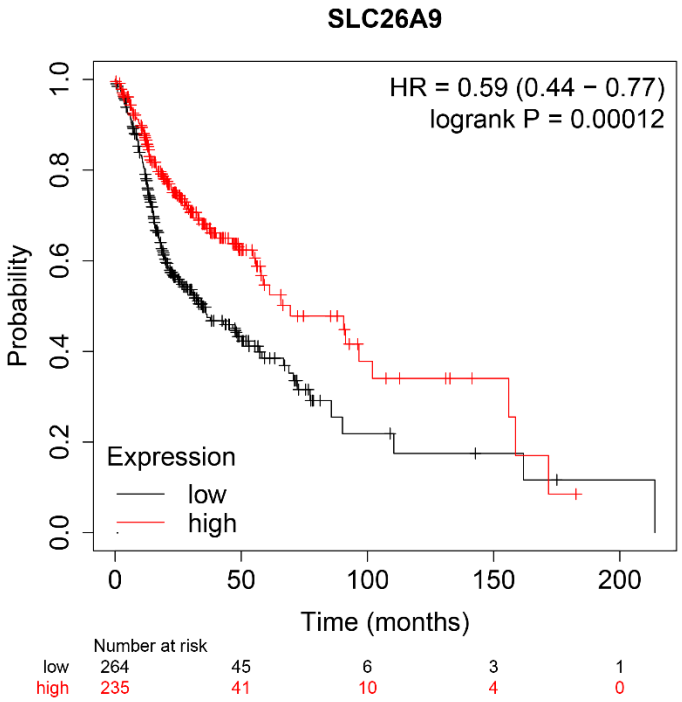

Supplementary Figure 10. KM survival analysis of SLC26A9.

Supplementary Tables

Please browse Full Text version to see the data of Supplementary Tables 3, 4, 6.

Supplementary Table 1. The specific transcription factors for HNSCC.

regulon
CSDE1
ZNF207
LTF
YBX1
PITX1
TP63
NFE2L1
XBP1
HIF1A
KLF5
TSC22D1
MAZ
USF2
STAT1
EPAS1
NFE2L2
SFPQ
IRF6
EGR1
ID1
ATF4
BHLHE40
MYC
HMGA1
SSRP1
ARID5B
ETS2
ZNF385A
HMGB2
PHB
STAT3
CNBP
FOS
JUNB
FOSL1
JUN
MAF1
ZFP36L1
LITAF
HMGB1
SREBF2

ATF6B
NME2
ZEB2
EBF1
FOXP3
TP53

Supplementary Table 2. The list of Mitophagy-Related Genes.

ATG12
ATG5
CSNK2A1
CSNK2A2
CSNK2B
FUNDC1
MAP1LC3A
MAP1LC3B
MFN1
MFN2
MTERF3
PGAM5
PINK1
PRKN
RPS27A
SQSTM1
SRC
TOMM20
TOMM22
TOMM40
TOMM5
TOMM6
TOMM7
TOMM70
UBA52
UBB
UBC
ULK1
VDAC1

Supplementary Table 3. Subtype differentially expressed genes based on limma algorithm.

Supplementary Table 4. Univariate COX regression analysis of subtype differential genes.

Supplementary Table 5. The result of Bootstrapping-based analysis.

	gene	times
1	GRHL3	1000
2	MS4A2	997
3	SCNN1B	996
4	ATP10B	995
5	A2ML1	992
6	TGM5	981
7	BNIPL	978
8	SASH1	977
9	ALOX12B	965
10	KRT80	893
11	PLA2G3	891
12	SPINK5	867
13	ZNF831	781
14	SLC26A9	749
15	LY6G6C	742
16	MASP1	722
17	MUC15	683
18	TMPRSS11D	675
19	FAM83C	649

Supplementary Table 6. The result of receptor ligand pairs between riskhighepi or risklowepi and others.